Article

53BP1-mediated recruitment of RASSF1A to ribosomal DNA breaks promotes local ATM signaling

Stavroula Tsaridou[1] , Georgia Velimezi[1,2] , Frances Willenbrock[3], Maria Chatzifrangkeskou[3,†], Waheba Elsayed[4], Andreas Panagopoulos[1,‡] , Dimitris Karamitros[5] , Vassilis Gorgoulis[2,6,7,8] , Zoi Lygerou[1] , Vassilis Roukos[1,4] , Eric O'Neill[3,*] & Dafni Eleftheria Pefani[1,**]

Abstract

DNA lesions occur across the genome and constitute a threat to cell viability; however, damage at specific genomic loci has a relatively greater impact on overall genome stability. The ribosomal RNA gene repeats (rDNA) are emerging fragile sites. Recent progress in understanding how the rDNA damage response is organized has highlighted a key role of adaptor proteins. Here, we show that the scaffold tumor suppressor RASSF1A is recruited to rDNA breaks. RASSF1A recruitment to double-strand breaks is mediated by 53BP1 and depends on RASSF1A phosphorylation at Serine 131 by ATM kinase. Employing targeted rDNA damage, we uncover that RASSF1A recruitment promotes local ATM signaling. RASSF1A silencing, a common epigenetic event during malignant transformation, results in persistent breaks, rDNA copy number alterations and decreased cell viability. Overall, we identify a novel role for RASSF1A at rDNA break sites, provide mechanistic insight into how the DNA damage response is organized in a chromatin context, and provide further evidence for how silencing of the RASSF1A tumor suppressor contributes to genome instability.

Introduction

DNA double-strand breaks (DSBs) are the most hazardous lesions arising in the genome of eukaryotic organisms that must be efficiently repaired to secure maintenance of genome integrity and survival. The two main pathways for DSB repair are Non-Homologous End Joining (NHEJ) in which the broken ends are directly ligated and Homologous Recombination (HR) which requires a non-damaged homologous sequence as a template, usually served by the sister chromatid (Jackson & Bartek, 2009; Gorgoulis *et al*, 2018). The latter process is considered to be error free; however, emerging evidence highlights that HR in clustered repetitive loci may be deleterious as it can lead to DNA repeat aberrations and/or chromosomal translocations (Mitrentsi *et al*, 2020).

The ribosomal RNA repeats (rDNA) that transcribe for the ribosomal RNA are organized in clusters at the Nucleolar Organizer Regions (NORs) at the short arms of the five acrocentric human chromosomes. Humans have around 300 rDNA repeats that contain a 13 Kb transcribed region and a 30 Kb Intergenic spacer (IGS). The rDNA repeats are transcribed by Polymerase I (Pol I) in a 47S pre-rRNA transcript that then is processed to 18S, 28S and 5.8S rRNAs. Due to recombinogenic instability of the rDNA repeats, there is a 10-fold variation in copy numbers among individuals in human populations (Stults *et al*, 2008; Gibbons *et al*, 2015). During malignant transformation, replication stress can lead to copy number alterations within the rDNA repeats that have been proposed to serve as a biomarker in therapy treatment or disease severity (Stults *et al*, 2009; Ide *et al*, 2010; Warmerdam *et al*, 2016; Wang & Lemos, 2017). Breaks that arise within the rDNA repeats have been

1 Department of Biology, School of Medicine, University of Patras, Patras, Greece
2 Biomedical Research Foundation of the Academy of Athens, Athens, Greece
3 Department of Oncology, University of Oxford, Oxford, UK
4 Institute of Molecular Biology (IMB), Mainz, Germany
5 Department of Physiology, School of Medicine, University of Patras, Patras, Greece
6 Laboratory of Histology and Embryology, Medical School, National and Kapodistrian University of Athens, Athens, Greece
7 Faculty of Biology, Medicine and Health, Manchester Academic Health Centre, University of Manchester, Manchester, UK
8 Ninewells Hospital and Medical School, University of Dundee, Dundee, UK
*Corresponding author. Tel: +44 1865617321; E-mail: eric.oneill@oncology.ox.ac.uk
**Corresponding author. Tel: +30 2610997619; E-mail: dpefani@upatras.gr
†Present address: Department of Biological Sciences, University of Cyprus, Nicosia, Cyprus
‡Present address: Department of Molecular Mechanisms of Disease, University of Zurich, Zurich, Switzerland

suggested to primarily undergo repair by NHEJ in the nucleolar interior. Persistent breaks relocate to the nucleolar periphery where they get access to the HR machinery, whilst the role of alternative end joining pathways that make use of homologous sequences next to the break site and are considered highly mutagenic, in rDNA repair has not yet been assessed (Harding *et al*, 2015; van Sluis & McStay, 2015; Warmerdam *et al*, 2016; Warmerdam & Wolthuis, 2019). Break relocation at the periphery serves to separate rDNA that originates from different chromosomes, which has been proposed to prevent interchromosomal recombination and is driven by nucleolar segregation (Floutsakou *et al*, 2013; van Sluis & McStay, 2015). These structural changes involve the merge of the fibrillar center (FC) and dense fibrillar component (DFC) of the nucleoli in a bipartite cap-like structure in the nucleolar periphery where rDNA HR repair takes place. Several studies have proposed that nucleolar segregation is driven by ATM-dependent transcriptional inhibition in the nucleoli (Kruhlak *et al*, 2007; Larsen *et al*, 2014; Harding *et al*, 2015; van Sluis & McStay, 2015; Pefani *et al*, 2018); however, more recent findings suggest that nucleolar segregation may be transcription-independent involving forces arising from Nuclear Envelope invaginations and the actin network (Marnef *et al*, 2019).

Emerging data show that the recombinogenic nature, high transcriptional activity, formation of secondary structures, and clustering of repeats that are localized in different chromosomes constitute the nucleolus a potential hot spot of genomic instability (Lindstrom *et al*, 2018). Therefore, to avoid the toxic effects of rDNA breaks, the nucleolar DNA damage response has evolved certain features including Polymerase I (Pol I) inhibition, dedicated adaptor proteins, chromatin modifications, and structural changes to achieve efficient break repair (Kruhlak *et al*, 2007; Larsen *et al*, 2014; van Sluis & McStay, 2015; Pefani *et al*, 2018; Korsholm *et al*, 2019; Mooser *et al*, 2020).

RASSF1A is a small tumor suppressor scaffold that we and others have shown to regulate Hippo pathway activity in the presence of genotoxic stress (Pefani & O'Neill, 2016). RASSF1A undergoes frequent promoter methylation early during malignant transformation, which has been linked with early cancer onset and/or worse disease outcome, indicating that the scaffold could be an attractive biomarker (Grawenda & O'Neill, 2015). We previously described the central kinase of the Hippo signaling cascade, MST2, as part of the nucleolar DNA damage response limiting Pol I transcription via phosphorylation of nucleolar chromatin (phosphorylation of H2B at Serine 14) upon double-strand break (DSB) formation in rDNA (Pefani *et al*, 2018). We showed that MST2 activity depends on RASSF1A. RASSF1A is phosphorylated by ATM/ATR kinases at Serine 131 leading to RASSF1A dimerization and orientation of the associated MST2 monomers to allow the stimulation of kinase activity (Hamilton *et al*, 2009; Pefani *et al*, 2014). Both RASSF1A and the MST2 kinase are present in the nucleolar fraction independently of damage; however, MST2 activation and subsequent H2B phosphorylation depend on ATM activity. H2B-pS14 was found in the nucleolar interior indicating that MST2 activity is not necessary for HR-mediated break repair at nucleolar cap located rDNA breaks (Pefani *et al*, 2018).

Herein, we characterize a previously unknown role of the RASSF1A scaffold at the sites of damage. We identify endogenous RASSF1A in a subset of breaks and characterize the scaffold's recruitment to rDNA breaks. Employing targeted damage at rDNA, we identify a novel interaction between RASSF1A and 53BP1 adaptor that mediates RASSF1A recruitment to the break sites. 53BP1 is known to promote local ATM signal amplification within damaged repetitive heterochromatic elements. We find here that 53BP1 is also necessary for local ATM signal establishment at damaged nucleoli and that the RASSF1A scaffold facilitates this role. RASSF1A downregulation results in compromised local ATM signaling, persistent breaks, and decreased cell viability. Moreover, *in vitro* and patient derived data show that compromised break repair upon RASSF1A silencing results in rDNA copy number discrepancies. We propose a model in which RASSF1A acts as a scaffold during initial nucleolar DNA damage response promoting H2BS14 phosphorylation to silence Pol I, via MST2, at the nucleolar interior and subsequently translocates with rDNA breaks to nucleolar caps in a 53BP1-dependent manner, to facilitate rDNA break repair. This study provides the first data for direct recruitment of the endogenous scaffold to the sites of damage and offers further mechanistic insight into how RASSF1A participates in the DNA damage response in a chromatin context.

Results

RASSF1A is localized at the sites of DNA damage

RASSF1A scaffold is one of the most common epigenetically inactivated genes in human malignancies due to promoter methylation (Grawenda & O'Neill, 2015; Dubois *et al*, 2019). RASSF1A is a tumor suppressor known to regulate the Hippo signaling cascade in response to genotoxic stress. RASSF1A-mediated activation of MST2 (hippo) promotes stalled replication fork protection (Pefani *et al*, 2014), apoptosis via the YAP transcriptional coactivator (Hamilton *et al*, 2009) and regulates Pol I transcriptional activity upon rDNA DSB formation (Pefani *et al*, 2018). RASSF1A is also involved in the repair of UV-induced DNA damage independently of Hippo via interaction with the XPA protein (Donninger *et al*, 2015). We looked for endogenous RASSF1A localization after exposure to ionizing radiation (γIR) and identified the scaffold co-localizing with γH2AX foci at the sites of damage (Figs 1A and EV1A and C). RASSF1A foci become evident between 30 min and 1 h post-irradiation and are no longer detectable 24 h after exposure, when break repair is completed (Fig 1B). To our knowledge, this is the first report of the endogenous protein being recruited to the sites of damage. We also observed RASSF1A recruitment to double-strand breaks induced by the radiomimetic agent Neocarzinostatin (NCS) and at micro laser-generated sites of damage (Figs 1E and EV1F and G). In contrast to UV laser-induced damage where the scaffold is recruited throughout the lesion (Fig EV1G), in γIR or NCS induced DNA breaks, RASSF1A is located only in a fraction of γH2AX foci (Figs 1A and EV1B), that could be explained by a spatial preference in recruitment. Closer examination of the distribution of RASSF1A foci shows that a significant fraction of RASSF1A lies at nucleoli boundaries where rDNA breaks relocate for HR-mediated repair (Figs 1C–E and EV1D–F). Moreover, when we measured the distance of RASSF1A foci from fibrillarin marked nucleoli, we found that RASSF1A^{+ve}/γH2AX^{+ve} foci are located closer to the nucleoli compared with the RASSF1A^{-ve}/γH2AX^{+ve} (Fig 1E). To further
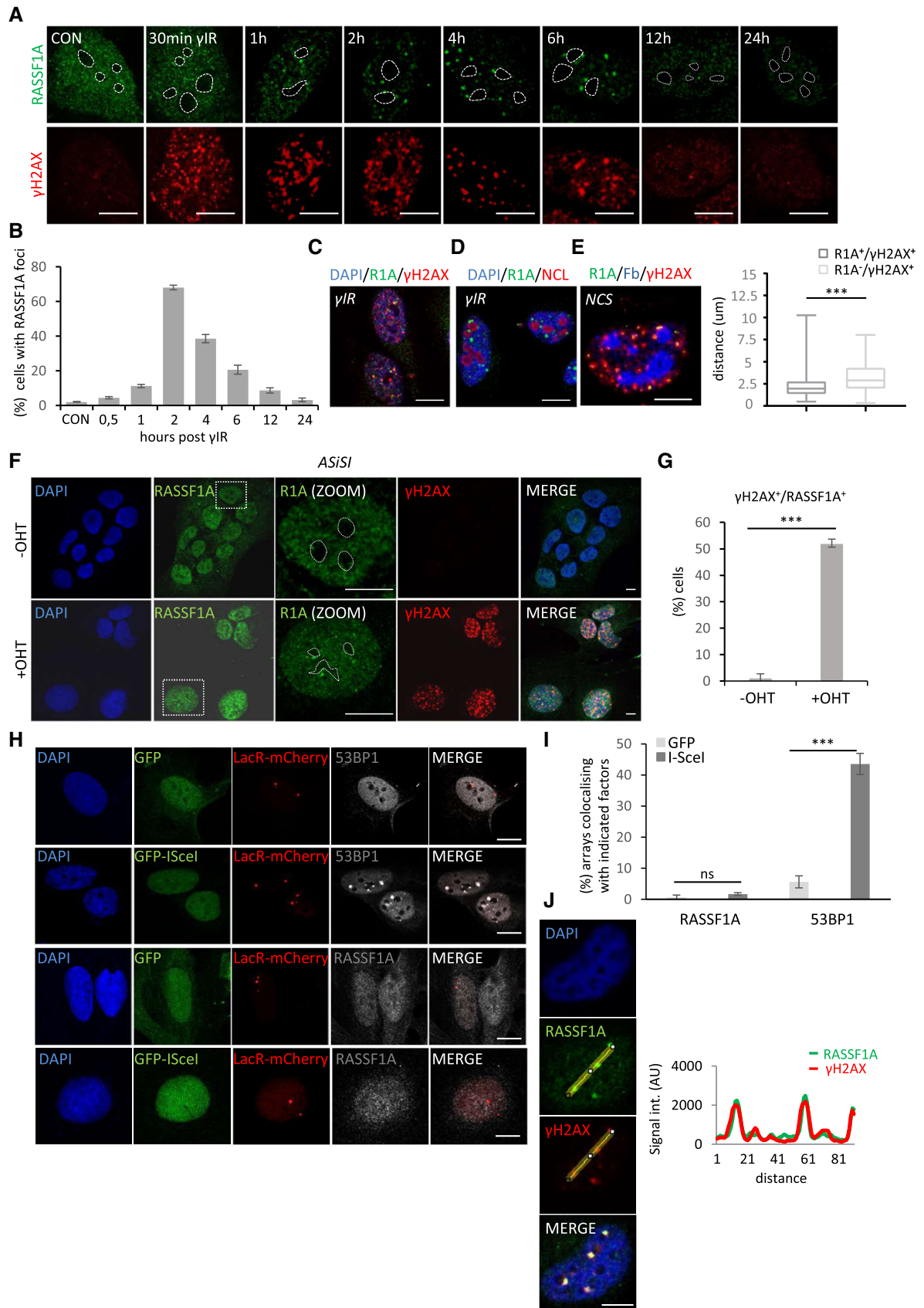
Figure 1.

Figure 1.   RASSF1A recruitment to double-strand breaks.

A   HeLa cells were exposed to 5 Gy ionizing radiation (γIR), collected at the indicated time points and stained for RASSF1A and γH2AX. Images for representative intra-nuclear RASSF1A foci distribution are shown. Nucleolar boundaries are marked with dashed lines.

B   Quantification of the number of cells with RASSF1A foci at the time points presented in (A). Error bars represent standard deviation and derive from three independent experiments.

C   HeLa cells were treated with 5 Gy γIR and 2 h posttreatment fixed and stained with the indicated antibodies.

D   HeLa cells were irradiated with 5 Gy and 2 h posttreatment stained for RASSF1A (R1A) and NUCLEOLIN (NCL).

E   HeLa cells were treated with 50 ng/ml NCS for 30 min, washed and 2 h later fixed and stained with the indicated antibodies. The distance of RASSF1A$^+$/γH2AX$^+$ foci or RASSF1A$^-$/γH2AX$^+$ foci to the closest nucleolus (based on Fibrillarin (Fb) staining) was measured. Middle line represents the median and the boxes 25th and 75th percentiles. The whiskers mark the smallest and largest values.

F   AsiSI expression in U2OS cells was induced by OHT and cells were stained for RASSF1A and γH2AX. Boxed areas are shown in higher magnification. Nucleolar boundaries are marked with dashed lines.

G   Quantification of the number of cells with RASSF1A foci in (F). Error bars represent standard deviation and derive from three independent experiments.

H   U2OS cells with stable integration of a Lac operator (LacO) sequence adjacent to an I-SceI endonuclease site were transfected with Lac Repressor (LacR)-mCherry and GFP or GFP-NLS-HA-I-SceI. 24 h post-transfection cells were fixed and stained for 53BP1 or RASSF1A.

I   Quantification of the LacO arrays enriched for 53BP1 or RASSF1A in (H). Error bars represent standard deviation and derive from three independent experiments.

J   HeLa cells were transfected with I-PpoI endonuclease and stained for RASSF1A and γH2AX. Fluorescence intensity profiles of RASSF1A (green) and γH2AX (red) signals across the HeLa nuclei are shown. Position of line scan indicated by the yellow line.

Data information: DNA was stained with DAPI. Scale bars = 10 μm. *P*-values in (B, G and I) were calculated using two-tailed Student's *t*-test. *P*-value in (E) was calculated using a Mann–Whitney test. * Indicates *P* = 0.05–0.01, ** indicates *P* = 0.01–0.001, *** indicates *P* ≤ 0.001.

assess the recruitment of the scaffold to the damaged rDNA loci, we used a cell line with inducible expression of the AsiSI endonuclease. AsiSI has several recognition sites within the human genome (Clouaire *et al*, 2018) and one of those is located at the 5' EST of the rDNA repeat. Breaks at the 5' EST of the rDNA repeat induced by AsiSI ectopic expression were recently shown to induce nucleolar segregation and movement of the rDNA breaks to the nucleolar periphery (Marnef *et al*, 2019). Interestingly, upon AsiSI expression, we observed RASSF1A recruitment mostly to γH2AX foci that are localized at the nucleolar caps indicating preferential recruitment of the scaffold at the rDNA breaks (Fig 1F and G); however, recruitment to other sites also takes place. To further examine whether there is a specificity in RASSF1A recruitment, we employed a Lac-repressor/operator-tethering system which consists of approximately 10 kb tandem arrays of the Lac operator (LacO) sequence adjacent to an I-SceI endonuclease site stably integrated into human U2OS cells at two random different chromosomal locations (Burgess *et al*, 2014). Expression of the Lac Repressor (LacR) fused with a fluorescent protein marks the LacO repeats in the vicinity of the I-SceI site. Upon expression of GFP-I-SceI, we observed increased 53BP1 accumulation at the I-SceI containing arrays (marked by LacR-mCherry) (Fig 1H and I); however, recruitment of RASSF1A was not evident under these conditions (Fig 1H and I). These findings are in agreement with RASSF1A being recruited to a subset of breaks possibly dictated by the chromatin environment.

Given the frequent localization of RASSF1A foci in proximity to the nucleolar periphery, we reasoned that rDNA breaks could be one of RASSF1A recruitment sites upon induction of damage. Given the increasing evidence for rDNA fragility and the contribution of rDNA damage in genomic instability (Lindstrom *et al*, 2018), we decided to get a better insight into whether RASSF1A is involved in rDNA break repair, employing the I-PpoI endonuclease to enrich for double-strand breaks at rDNA loci. As it has been previously described, I-PpoI recognizes a sequence within the 28S-rDNA coding region of each of the approximately 300 rDNA repeats and a limited number of other sites in the human genome (van Sluis & McStay, 2015). In agreement with previous reports, mRNA transfection of V5 tagged I-PpoI results in relocation of rDNA breaks to the

nucleolar periphery, formation of γH2AX-positive nucleolar caps and downregulation of Polymerase I transcriptional activity, whereas a catalytically inactive version of I-PpoI (H98A) does not result in rDNA DSBs (Fig EV1H–J). Indeed, upon induction of rDNA breaks and nucleolar cap formation, we observed robust recruitment of RASSF1A scaffold to γH2AX-positive nucleolar caps (Fig 1J). Overall, we find endogenous RASSF1A at a fraction of breaks with evidence supporting recruitment to rDNA sites.

RASSF1A is recruited to rDNA DSBs

To acquire a better understanding of RASSF1A temporal recruitment to rDNA breaks, we performed a time course after I-PpoI induction with the early marker of rDNA DSBs and upstream regulator of the nucleolar DNA damage response, NBS1 (Korsholm *et al*, 2019). RASSF1A microfoci are evident from 1 h post I-PpoI mRNA transfection when nucleolar cap formation starts in a small fraction of cells. Robust RASSF1A staining is observed when nucleolar caps establish between 2 and 6 h post I-PpoI transfection and RASSF1A foci disappear 24 h post I-PpoI transfection when the majority of breaks have been repaired and cells do not exhibit nucleolar NBS1 staining (Fig 2A and B). A similar analysis in different cell lines and with other markers known to localize at the rDNA breaks showed that RASSF1A co-localizes with the γH2AX mark and 53BP1 protein at the nucleolar caps and is in proximity with UBF and RPA (Fig EV2A–C). We previously showed that there is an endogenous nucleolar fraction of RASSF1A (Pefani *et al*, 2018), and while the formation of microfoci is evident in the nucleolar interior early after induction of rDNA breaks, we only observe robust recruitment to nucleolar caps where breaks relocate for HR-mediated repair (Fig EV2D). RASSF1A recruitment was also observed in cells with CRISPR/Cas9 induced breaks within the IGS spacer (Fig EV2E), indicating that RASSF1A accumulates at rDNA breaks independent of the break site. When we treated cells with the polymerase I inhibitor CX-5461 which results in rDNA breaks through increasing replication stress in rDNA (Sanij *et al*, 2020), we similarly observed RASSF1A recruitment to 53BP1^{+ve} nucleolar caps (Fig EV2F). To assess potential cell cycle dependency in RASSF1A recruitment to

rDNA DSBs, we co-stained cells with Cyclin A, a marker of S/G2 phases. RASSF1A is recruited at rDNA DSBs independently of the cell cycle stage (Fig EV2G and H). We recently reported that there is a fraction of RASSF1A at the nuclear envelope (NE), where it

facilitates nucleocytoplasmic actin transport (Chatzifrangkeskou et al, 2019). Methanol fixation facilitates the visualization of NE bound proteins and shows reduced pools of RASSF1A at the NE (LAMIN A/C^{+ve}) upon I-PpoI expression indicating that recruitment
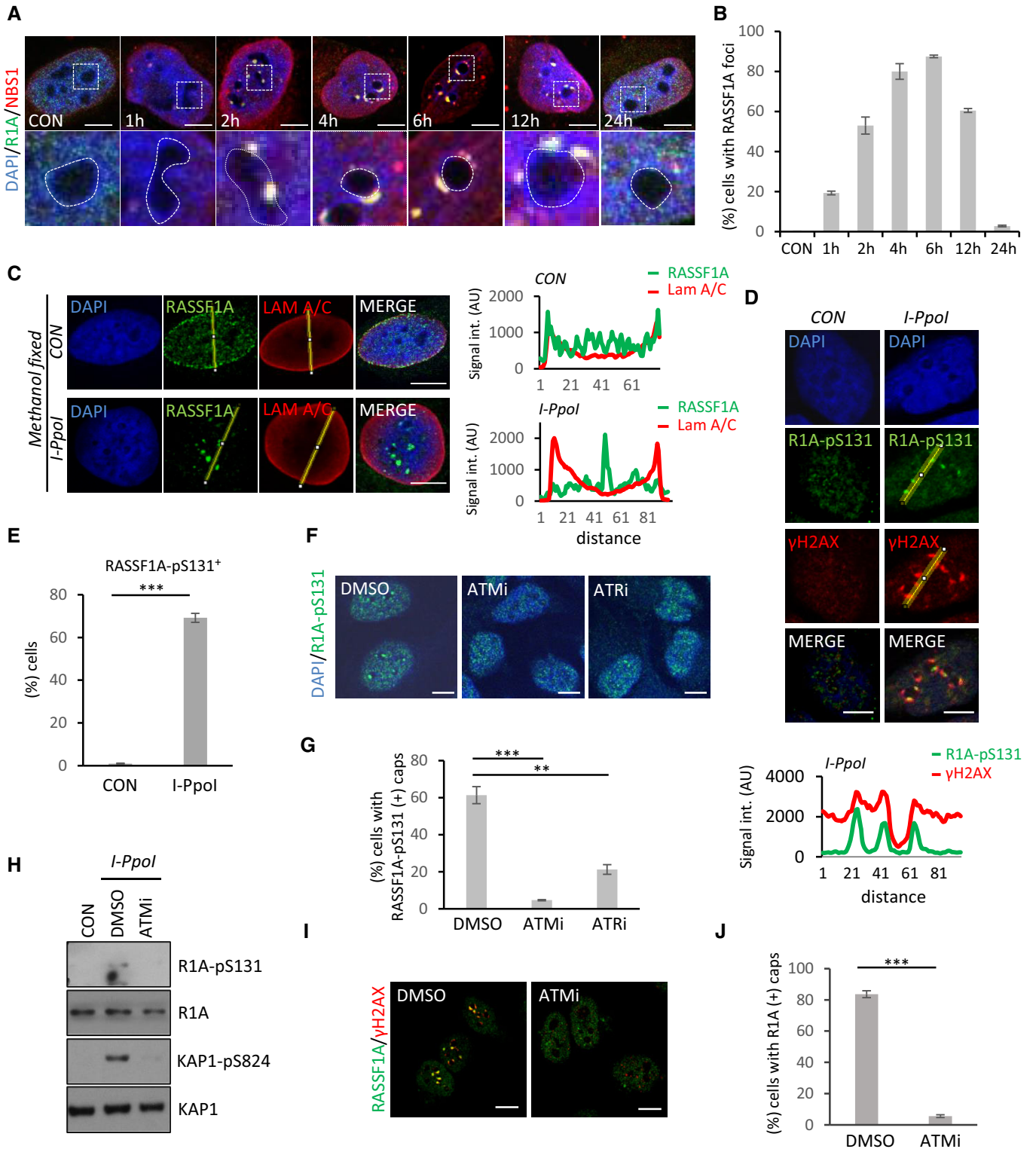
Figure 2.

Figure 2. Phosphorylated RASSF1A at Serine 131 localizes at the rDNA DSBs.

A HeLa cells were transfected with I-PpoI mRNA and collected at the indicated time points. Cells were co-stained for RASSF1A (R1A) and NBS1. Boxed areas are shown in higher magnification. Nucleolar boundaries are marked with dashed lines.

B Quantification of (A). Error bars represent standard deviation and derive from three independent experiments.

C Assessment of RASSF1A localisation after induction of rDNA DSBs using the I-PpoI endonuclease in methanol fixed HeLa cells. Fluorescence intensity profile of RASSF1A (green) and LAMIN A/C (red) signals across the HeLa nuclei in the presence and absence of rDNA DSBs in control and I-PpoI treated cells. Position of line scan indicated by the yellow line.

D HeLa cells were transfected with the I-PpoI mRNA and 6 h later stained for RASSF1A-pS131 (R1A-pS131) and γH2AX. Fluorescence intensity profile of RASSF1A-pS131 (green) and γH2AX (red) signals across the HeLa nuclei are shown. Position of line scan indicated by the yellow line.

E Quantification of cells with RASSF1A-pS131-positive nucleolar caps 6 h post-I-PpoI transfection. Error bars represent standard deviation and derive from three independent experiments. Representative images are shown in Fig EV3A.

F HeLa cells were treated with the ATMi or ATRi prior to transfection with I-PpoI mRNA. 6 h post-mRNA transfection cells were stained for RASSF1A-pS131 (R1A-pS131).

G Quantification of (F). Error bars represent standard deviation and derive from three independent experiments.

H HeLa cells were treated or not with ATM inhibitor (ATMi) followed by I-PpoI mRNA transfection and 6 h later cell lysates were analyzed by Western blot with the indicated antibodies.

I HeLa cells were treated or not with ATMi followed by I-PpoI mRNA transfection and 6 h later cells were fixed and RASSF1A recruitment to rDNA DSBs was assessed.

J Quantification of (I). Error bars represent standard deviation and derive from three independent experiments.

Data information: DNA was stained with DAPI. Scale bars = 10 μm. *P*-values in (E, G and J) were calculated using two-tailed Student's *t*-test. * Indicates $P = 0.05–0.01$, ** indicates $P = 0.01–0.001$, *** indicates $P \leq 0.001$.
Source data are available online for this figure.

from the nuclear envelope to the rDNA break sites occurs in response to damage (Fig 2C). Taken together, this data highlight that RASSF1A is recruited to breaks within the rDNA repeats independently of break site, mechanism of rDNA insult or stage of the cell cycle.

rDNA damage results in break localized RASSF1A-pS131

ATM has a central role in nucleolar DNA damage response promoting Pol I inhibition, nucleolar segregation, end resection and rDNA DSB repair, while recent studies showed that the related ATR kinase also contributes to the rDNA break response (Kruhlak *et al*, 2007; Harding *et al*, 2015; Pefani *et al*, 2018; Korsholm *et al*, 2019; Mooser *et al*, 2020). Moreover, RASSF1A is a target of both ATM and ATR kinases at Serine 131 (Hamilton *et al*, 2009; Pefani *et al*, 2014). Therefore, we looked for RASSF1A phosphorylation at Serine 131 (RASSF1A-pS131) upon rDNA DSB induction. We found that I-PpoI induced damage resulted in increased RASSF1A-pS131 levels and accumulation of the phosphorylated protein at the γH2AX marked rDNA DSBs (Figs 2D and E, and EV3A). Inhibition of ATM or ATR kinases results in decreased establishment of RASSF1A-pS131 at the sites of rDNA breaks (Fig 2F and G) with ATM inhibition having a more profound effect. Western blot analysis showed that rDNA damage results in an ATM-dependent increase of RASSF1A-pS131, whilst total RASSF1A protein levels are not affected (Fig 2H). Inhibition of ATM kinase also resulted in abrogation of RASSFS1A foci formation in damaged nucleoli (Fig 2I and J). Once again, ATM inhibition had a more profound effect on RASSF1A recruitment compared to inhibition of ATR activity (Fig EV3B and C). In the presence of ATM inhibitor, the RASSF1A NE-associated fraction stays intact, further supporting that the NE-associated fraction of the scaffold is recruited to rDNA DSBs (Fig EV3D). Knockdown of Treacle, an upstream adaptor protein that regulates ATR activation at the damaged nucleoli (Mooser *et al*, 2020), also results in abrogation of RASSF1A recruitment (Fig EV3E and F). Overall, the above data highlight that RASSF1A-pS131 is recruited to the rDNA damage sites and ATM signaling is necessary for RASSF1A recruitment at rDNA breaks.

53BP1 interacts with RASSF1A to mediate recruitment to rDNA breaks

Closer examination of RASSF1A sub-nucleolar cap distribution shows that RASSF1A co-localizes with 53BP1 protein and is found in proximity but not fully co-localizing with RPA, BRCA1 or MRE-11 factors, following the intra-nucleolar distribution of 53BP1 (Fig 3A and B). Despite the lack of evidence for NHEJ at nucleolar caps, we and others observe robust recruitment of 53BP1, its upstream recruitment regulator RNF8 (Schwertman *et al*, 2016) and partner RIF1 (Chapman *et al*, 2013) at the nucleolar caps of damaged nucleoli (Fig EV3G). Given the colocalization between RASSF1A and 53BP1, we next sought to address whether 53BP1 is involved in the establishment of RASSF1A foci. When 53BP1 or its upstream regulator RNF8 expression was knocked down, RASSF1A recruitment to rDNA breaks was significantly perturbed (Fig 3C–F). Lack of RASSF1A recruitment under these conditions is not a consequence of defective segregation, as knockdown of 53BP1 or RNF8 does not affect cap formation (Fig EV3H and I). Moreover, Pol I transcriptional inhibition is retained in damaged nucleoli of 53BP1 knocked down cells (Fig EV3J and K), indicating that 53BP1 is not involved in nucleolar transcriptional regulation upon induction of rDNA DSBs.

Given the dependency of 53BP1 recruitment on γH2AX (Kleiner *et al*, 2015), we questioned whether loss of RASSF1A recruitment upon ATM kinase inhibition is attributed to loss of 53BP1 establishment. In agreement with previous observations (Harding *et al*, 2015), we find robust 53BP1 recruitment to damaged nucleoli upon ATM inhibition potentially due to residual ATR-mediated γH2AX establishment (Fig EV4A and B). Inhibition of ATM signaling or depletion of the 53BP1 adaptor also resulted in reduced RASSF1A foci formation in irradiated cells, indicating that RASSF1A recruitment dependency on the ATM-53BP1 axis is independent of the source of damage (Figs 3G and H, and EV4C). Given that downregulation of RNF8 results in loss of RASSF1A recruitment to damaged nucleoli (Fig 3E and F), we also assessed the effect of BRCA1 knockdown, as BRCA1 is also recruited to the sites of damage via RNF8 (Mailand *et al*, 2007).
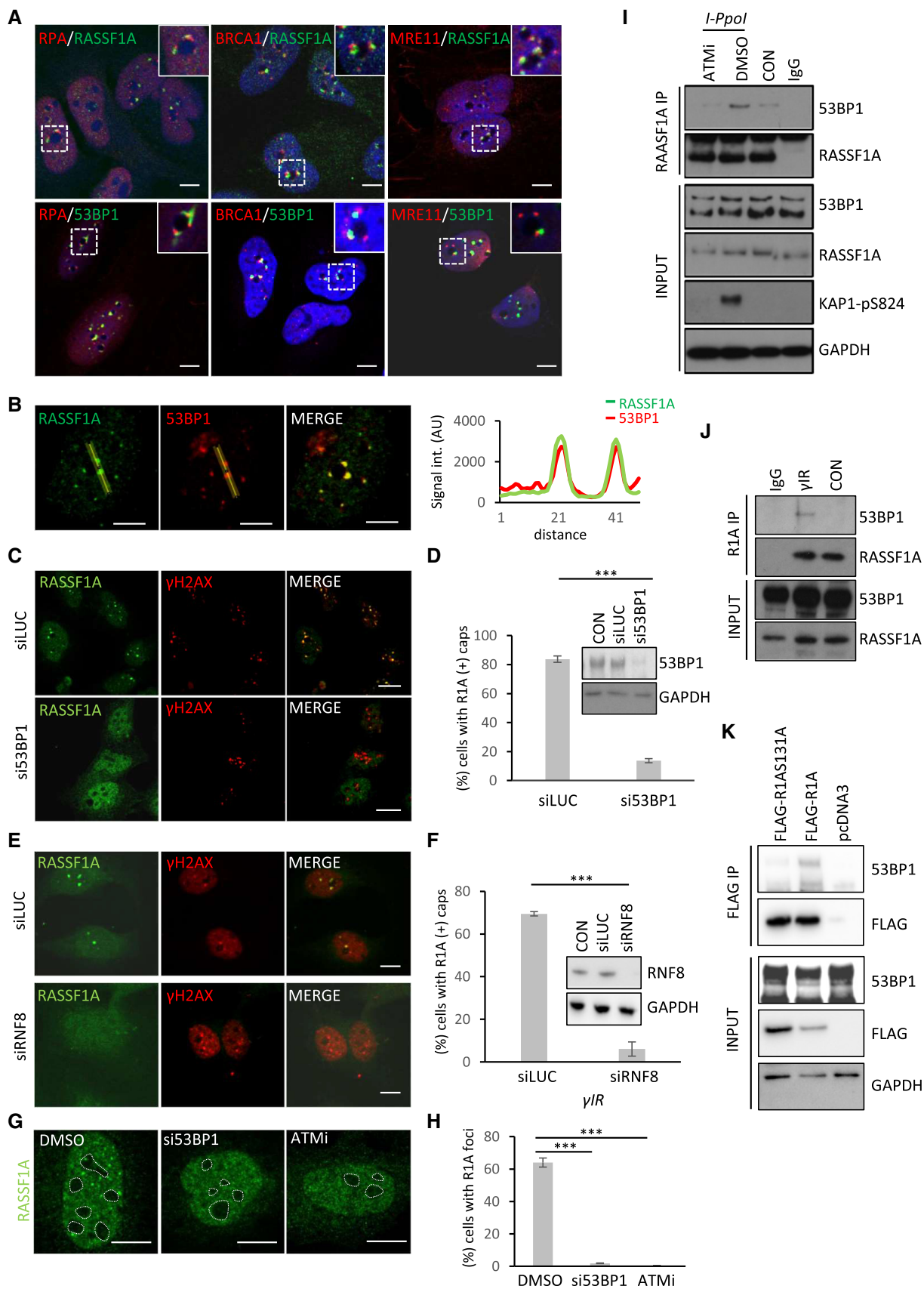
Figure 3.

Figure 3. RASSF1A recruitment to rDNA DSBs depends on 53BP1.

A HeLa cells with I-PpoI induced rDNA breaks were stained with the indicated antibodies. Intra-nucleolar cap localization for RASSF1A and 53BP1 in correlation with other proteins was accessed. Boxed areas are shown in higher magnification.

B HeLa cells were transfected with I-PpoI mRNA and stained for RASSF1A and 53BP1. Fluorescence intensity profiles of RASSF1A (green) and 53BP1 (red) signals across the HeLa nuclei are shown. Position of line scan indicated by the yellow line.

C HeLa cells were treated with siRNAs against LUCIFERASE (siLUC) or 53BP1 (si53BP1), 48 h later transfected with I-PpoI mRNA, fixed and stained for RASSF1A (R1A) and γH2AX.

D Quantification of (C) and Western blot analysis from siLUCIFERASE (siLUC) or si53BP1-treated cells with the indicated antibodies. Error bars represent standard deviation and derive from three independent experiments.

E HeLa cells were treated with siRNAs against LUSIFERASE (siLUC) or RNF8 (siRNF8), 48 h later transfected for I-PpoI mRNA, fixed and stained for RASSF1A and γH2AX.

F Quantification of (E) and Western blot analysis from siLUCIFERASE (siLUC) or siRNF8-treated cells with the indicated antibodies. Error bars represent standard deviation and derive from three independent experiments.

G HeLa cells were treated with siRNA against 53BP1, or an ATM inhibitor (ATMi) followed by 5 Gy of ionizing radiation (γIR). Cells were fixed 2 h posttreatment and stained for RASSF1A. Nucleolar boundaries are marked with dashed lines.

H Quantification of cells with RASSF1A foci in (G). Error bars represent standard deviation and derive from three independent experiments.

I Western blot analysis from total cell extracts with the indicated treatments and RASSF1A immuneprecipitates (IPs) with the indicated antibodies. IgG immunoprecipitation served as a control.

J Western blot analysis from total cell extracts and RASSF1A immunoprecipitates with the indicated treatments with the indicated antibodies. IgG immunoprecipitation served as a control.

K U2OS cells were transfected with FLAG-RASSF1A (FLAG-R1A), FLAG-RASSF1A131A (FLAG-R1A131A) or pcDNA3 and 24 h later transfected with the I-PpoI mRNA. Cell lysates were subjected to immunoprecipitation with a FLAG-tag antibody. Western blot analysis of total cell extracts and the IPs is shown.

Data information: DNA was stained with DAPI. Scale bars = 10 μm. *P*-values in (D, F and H) were calculated using two-tailed Student's *t*-test. * Indicates $P = 0.05$–0.01, ** indicates $P = 0.01$–0.001, *** indicates $P \leq 0.001$.
Source data are available online for this figure.

Depletion of BRCA1 (Fig EV4D) does not affect the number of cells with RASSF1A-positive caps (Fig EV4E and F). Whilst the number of cells with 53BP1-positive nucleolar caps is not altered upon BRCA1 downregulation (Fig EV4G and H), the intensity of nuclear 53BP1 signal is augmented (Fig EV4G and I), indicating increased recruitment to rDNA breaks, in agreement with previous observations for irradiation-induced damage (Daley & Sung, 2014).

We next assessed whether 53BP1-mediated RASSF1A recruitment is via protein–protein interaction. Indeed, we were able to observe co-immunoprecipitation (IP) (Fig 3I and J) that was significantly induced in response to treatment with ionizing radiation (Fig 3J) or induction of rDNA DSBs with the I-PpoI endonuclease (Fig 3I). Furthermore, ATM inhibition resulted in decreased RASSF1A-53BP1 interaction (Fig 3I). To examine whether this is a consequence of loss of the ATM-dependent RASSF1A phosphorylation, we looked for interaction between 53BP1 with FLAG-tagged RASSF1A or a phospho-site mutant. 53BP1 was significantly reduced in FLAG-RASSF1AS131A IP, suggesting that interaction depends on RASSF1A phosphorylation by ATM (Fig 3K). 53BP1 BRCT domain is not necessary for interaction with RASSF1A; however, the N-terminus,which is known to undergo phosphorylation by ATM and ATR in multiple sites to mediate interaction with PTIP and RIF1 (Mirman & de Lange, 2020), is required for interaction with the RASSF1A scaffold (Fig 4A). To further characterize 53BP1-RASSF1A interaction, we used a series of RASSF1A-truncated mutants to determine the domain responsible for the interaction. Full-length RASSF1A (1–340) associates with 53BP1, but derivatives lacking the C-terminal SARAH domain (1–288 and 120–288), a coiled-coil domain known to also mediate interaction with MST2 kinase (Matallanas et al, 2007) did not co-precipitate with 53BP1 (Fig 4B). Therefore, we identified a novel genotoxic-stress induced interaction between 53BP1 and RASSF1A that depends on RASSF1A phosphorylation by ATM and is necessary for recruitment of the scaffold to rDNA DSBs.

RASSF1A facilitates the establishment of the nucleolar DNA damage response

We previously showed that RASSF1A is involved in MST2 activation for the establishment of nucleolar H2BS14 phosphorylation early in response to induction of damage (Pefani et al, 2018). In agreement with our previous findings, we observed increased nucleolar 5-EU incorporation in RASSF1A knockdown cells (Fig EV4J–L). Given that RASSF1A is necessary for nucleolar MST2 activity phosphorylation of H2B at Serine 14 to facilitate Pol I transcriptional inhibition (Pefani et al, 2018), we looked whether RASSF1A depletion affects nucleolar segregation. Several studies have highlighted the link between transcriptional inhibition and nucleolar segregation; however, recent data suggest that the two processes may be uncoupled (Marnef et al, 2019; Fages et al, 2020). siRASSF1A-treated cells show a decrease in fully segregated nucleoli, with most of the cells presenting a partially segregated phenotype with formation of UBF condensates that do not fully move to the nucleolar exterior (Fig EV4M and N). Limited segregation was also reported in siMST2-treated cells, in agreement with RASSF1A-MST2 mediated Pol I transcriptional regulation being involved in nucleolar segregation (Pefani et al, 2018). Depletion of 53BP1 does not affect Pol I transcriptional shut down or cause nucleolar segregation defects (Fig EV3H–K), suggesting that RASSF1A recruitment to rDNA DSBs, which is compromised in 53BP1 knocked down cells, is not involved in the regulation of nucleolar segregation.

53BP1 was previously shown to act in local ATM signal amplification within heterochromatic repetitive elements to facilitate the phosphorylation of ATM substrates upon exposure to γIR to promote chromatin decondensation at the sites of damage (Baldock et al, 2015; DiTullio et al, 2002; Lee et al, 2010; Noon et al, 2010). Downregulation of 53BP1 also results in decreased ATM-pS1981 establishment at damaged rDNA repeats (Fig 4C and D). To examine whether 53BP1-mediated recruitment of RASSF1A could facilitate local ATM signal establishment, we knocked down RASSF1A
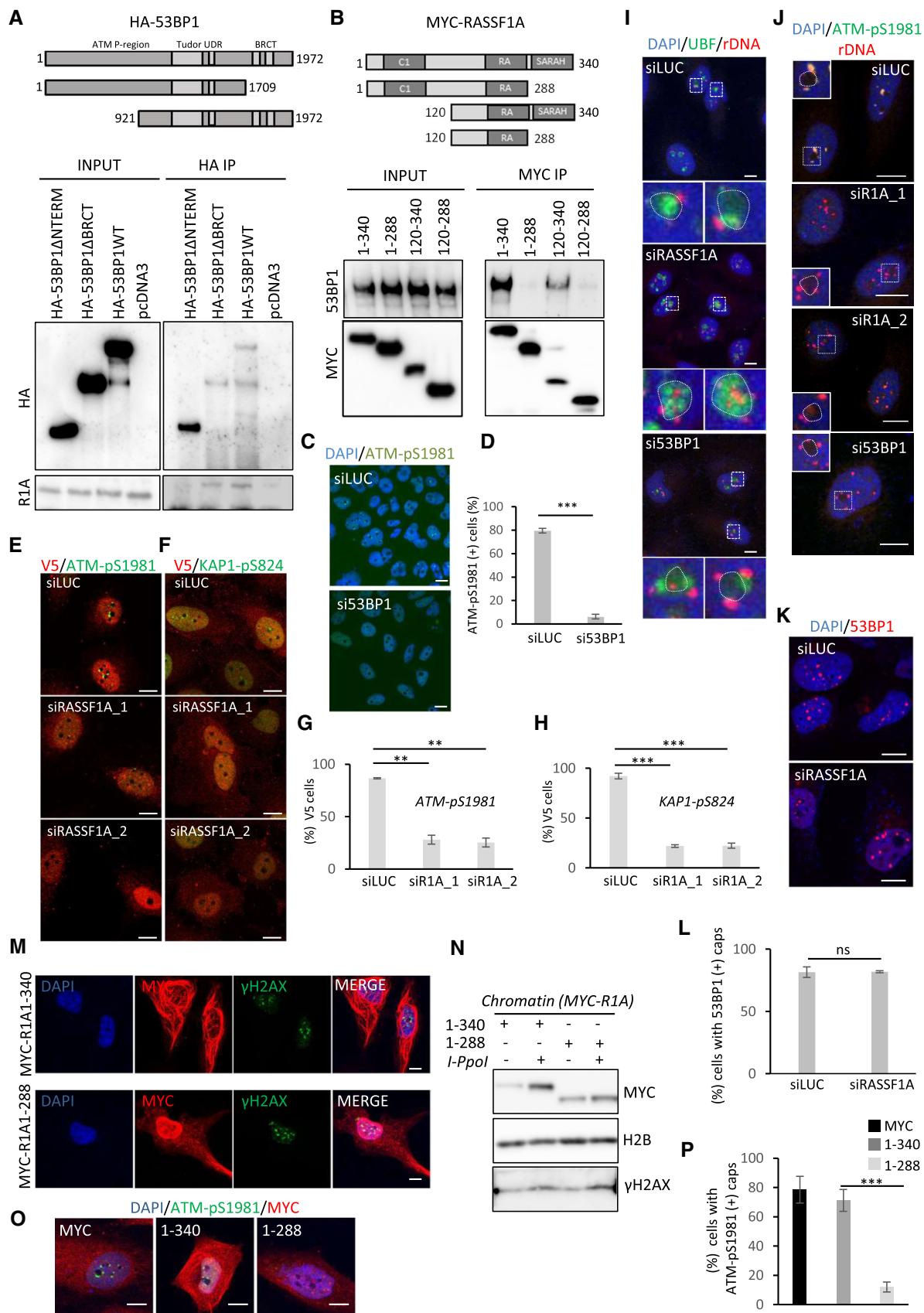
Figure 4.

Figure 4. RASSF1A depletion results in impaired rDNA damage response.

A   U2OS cells were transfected with either HA-53BP1WT (aa1–1972), HA-53BP1ΔBRCT (aa 1–1709), HA-53BP1ΔNterminus (aa 921–1972) or empty pcDNA3 vector and 24 h later transfected with I-PpoI mRNA. Cell lysates were subjected to immunoprecipitation with an HA tag antibody. Western blot analysis of total cell extracts and the IPs is shown.

B   U2OS cells were transfected with either full-length MYC-RASSF1A or with the indicated RASSF1A deletion mutants and 24 h later transfected with I-PpoI mRNA. Cell lysates were subjected to immunoprecipitation with a MYC-tag antibody. Western blot analysis of the total cell extracts and the IPs is shown.

C   HeLa cells were treated with siLUCIFERASE (siLUC) or si53BP1 and 48 h later transfected with I-PpoI mRNA and stained for ATM-pS1981.

D   Quantification of (C). Error bars represent standard deviation and derive from three independent experiments.

E–H HeLa cells were treated with siLUCIFERASE (siLUC) or two different siRNAs against RASSF1A (siR1A_1 and siR1A_2) and 48 h later cells were transfected with I-PpoI mRNA to induce rDNA DSBs. 6 h post-mRNA transfection, cells were stained for V5 to identify I-PpoI transfected cells and the other indicated antibodies. Representative images (E, F) and quantification based on staining (G, H) with the indicated antibodies are shown. Error bars represent standard deviation and derive from three independent experiments.

I   HeLa cells were treated with siLUCIFERASE (siLUC), siRASSF1A or si53BP1 and 48 h later transfected with the I-PpoI mRNA. Cells were fixed and underwent ImmunoFISH against UBF and an rDNA probe. Boxed areas are shown in higher magnification. Nucleolar boundaries are marked with dashed lines.

J   HeLa cells were treated with siLUCIFERASE (siLUC), siRASSF1A or si53BP1 and 48 h later transfected with the I-PpoI mRNA. Cells were fixed and underwent ImmunoFISH against ATM-pS1981 and an rDNA probe. Boxed areas are shown in higher magnification. Nucleolar boundaries are marked with dashed lines.

K   HeLa cells were treated with siLUCIFERASE (siLUC) or siRASSF1A followed by I-PpoI mRNA transfection. 6 h later, cells were stained for 53BP1.

L   Quantification of (K). Error bars represent standard deviation and derive from three independent experiments.

M   U2OS cells were transfected with MYC-RASSF1A (1–340) or a RASSF1A mutant that lacks the SARAH domain, MYC-RASSF1A (1–288). Cells were transfected with I-PpoI mRNA and stained with the indicated antibodies.

N   U2OS cells were transfected with MYC-RASSF1A (1–340) or MYC-RASSF1A (1–288). 24 h later cells were transfected with I-PpoI mRNA and harvested after 6 h. Cell lysates underwent cell fractionation and the chromatin-bound fraction was analyzed by western blot.

O   U2OS cells were treated with siLUC followed by transfection with MYC-tag or siRASSF1A followed by transfection with MYC-RASSF1A (1–340) or MYC-RASSF1A (1–288). 24 h later cells were transfected with I-PpoI mRNA and stained for MYC expression and ATM-pS1981.

P   Quantification of cells with ATM-pS1981 positive nucleolar caps in (O). Error bars represent standard deviation and derive from three independent experiments.

Data information: DNA was stained with DAPI. Scale bars = 10 μm. *P*-values in (D, G, H, L and P) were calculated using two-tailed Student's *t*-test. * Indicates $P = 0.05$–0.01, ** indicates $P = 0.01$–0.001, *** indicates $P \leq 0.001$.
Source data are available online for this figure.

and looked for ATM-pS1981 and the downstream target KAP1-pS824 (Fig 4E–H). Establishment of both markers was reduced at the nucleolar caps of siRASSF1A-treated cells, indicative of a defective spatial concentration of ATM activity similar to that observed upon 53BP1 depletion (Fig 4C and D). In agreement to what was previously observed for 53BP1 depleted cells in heterochromatin elements (Noon *et al*, 2010), total ATM occupancy of nucleolar caps of siRASSF1A treated cells was also decreased (Fig EV4O and P). Given the partial segregation phenotype of RASSF1A depleted cells (Fig EV4M and N), we wanted to further address whether the lack of ATM signal establishment is due to lack of rDNA break movement to the nucleolar periphery. We therefore performed rDNA ImmunoFISH using an rDNA-specific probe (van Sluis *et al*, 2016) and stained for UBF, a marker for nucleolar segregation (Fig 4I). In agreement with unperturbed formation of nucleolar caps in si53BP1-treated cells (Fig EV3H and I), we observed robust mobilization of rDNA in the nucleolar periphery (Figs 4I and EV4Q). rDNA mobilization was also evident in siRASSF1A-treated cells despite defective nucleolar segregation based on UBF staining (Figs 4I and EV4O). Moreover, in ImmunoFISH experiments where cells were stained for rDNA and ATM-pS1981, we observed lack of active nucleolar ATM despite rDNA exposure at the nucleolar exterior (Fig 4J). Knockdown of RASSF1A did not impact on 53BP1 establishment at nucleolar caps (Fig 4K and L), indicating that RASSF1A acts downstream of 53BP1.

We then sought to further characterize the RASSF1A mutant that lacks the SARAH domain and showed limited interaction with 53BP1 (Fig 4B). As widely observed for tubulin binding proteins, expression of exogenous RASSF1A results in significant association with the microtubule network (Rong *et al*, 2004) imposing technical difficulties in the imaging of the nuclear and chromatin-bound fractions (Fig 4M). In agreement with previously published data (El-

Kalla *et al*, 2010), we find that the RASSF1A mutant that lacks the SARAH domain exhibits enhanced nuclear localization; however, we did not observe any recruitment to nucleolar caps (Fig 4M). We also employed chromatin fractionation analysis and found that while full-length RASSF1A displays increased presence in the chromatin fraction of I-PpoI-treated cells compared with the control condition, the RASSF1A 1–288 mutant that lacks the SARAH domain is not equally enriched in chromatin upon rDNA damage (Fig 4N). Moreover, in contrast to full-length RASSF1A, when RASSF1A SARAH-deletion mutant is expressed in cells that were previously treated with siRNA against RASSF1A there is no re-establishment of ATM-pS1981 at nucleolar caps (Fig 4O and P).

Previous studies have reported that DNA end resection based on RPA foci formation in damaged rDNA, in contrast to other genomic loci, is placed downstream of ATM/ATR signaling (Korsholm *et al*, 2019; Mooser *et al*, 2020). We also observed loss of RPA establishment at nucleolar caps of damaged nucleoli upon inhibition of the ATM and ATR kinases (Figs 5A and EV4R). Loss of ATM and ATR activity also results in decreased formation of RAD51 nucleofilaments at nucleolar caps, in agreement with defective resection (Figs 5B and EV4S). RASSF1A knockdown phenocopies the effect of ATM inhibition on the establishment of RPA foci and RAD51 nucleofilaments at damaged nucleoli (Figs 5C–F). Moreover, reduced RPA phosphorylation (RPA-pS4/8 and RPA–pS33) was observed in I-PpoI-treated cells knocked down for RASSF1A (Fig 5G).

In contrast to ATM inhibition or RASSF1A downregulation, but in agreement with the well-established role of 53BP1 acting against DNA resection, depletion of 53BP1 resulted in an enhanced RPA signal (Fig 5H and I). Assessment of ssDNA with native BrdU staining also confirms that in contrast to downregulation of 53BP1, RASSF1A knockdown results in decreased ssDNA at nucleolar caps
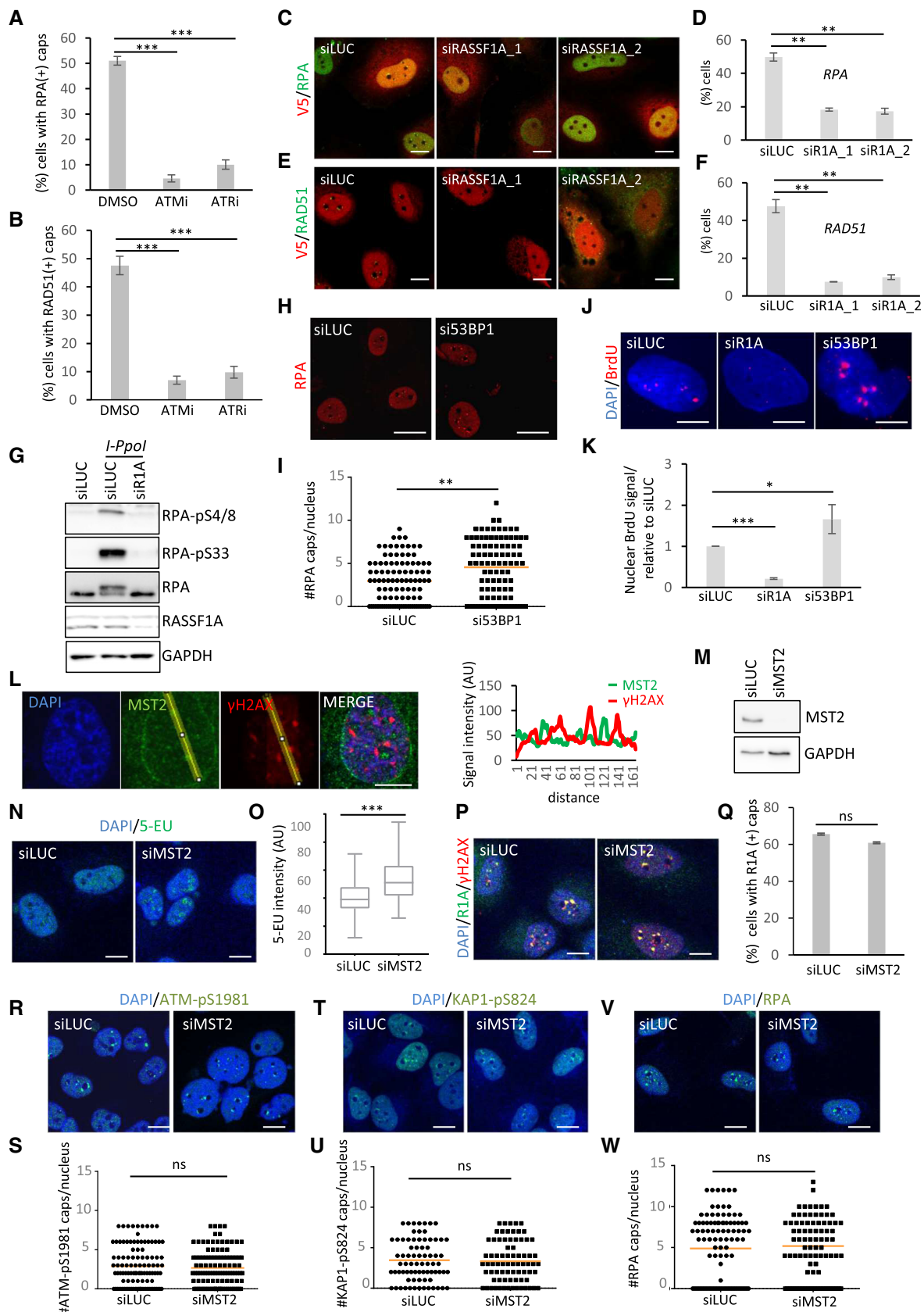
Figure 5.

◀

Figure 5. RASSF1A function at rDNA breaks is not mediated by MST2 kinase.

A HeLa cells were pretreated with the ATMi or ATRi prior to transfection with I-PpoI mRNA. Cells were stained for RPA and quantified. Representative images are shown in (Fig EV4R). Error bars represent standard deviation and derive from three independent experiments.

B HeLa cells were pretreated with the ATMi or ATRi prior to transfection with I-PpoI mRNA. Cells were stained for RAD51 and quantified. Representative images are shown in (Fig EV4S). Error bars represent standard deviation and derive from three independent experiments.

C–F HeLa cells were treated with siLUCIFERASE (siLUC) or two different siRNAs against RASSF1A (siR1A_1 and siR1A_2), and 48 h later, cells were transfected with I-PpoI mRNA to induce rDNA DSBs. 6 h post-mRNA transfection, cells were stained for V5 to identify I-PpoI transfected cells and the other indicated antibodies. Representative images (C, E) and quantification based on staining (D, F) with the indicated antibodies are shown. Error bars represent standard deviation and derive from three independent experiments.

G Western blot analysis from HeLa cell extracts treated with the indicated siRNAs with the indicated antibodies.

H Cells were treated with siLUCIFERASE (siLUC) or si53BP1 and 48 h later transfected with I-PpoI mRNA and stained for RPA.

I Quantification of (H). 107 values were analyzed in siLUC and 90 values were analyzed in si53BP1.

J U2OS cells were treated with siLUCIFERASE (siLUC), siRASSF1A (siR1A) or si53BP1, treated with 10 μM BrdU for 24 h prior to I-PpoI mRNA transfection. 6 h post I-PpoI treated cells were pre-extracted, fixed and stained for BrdU under non-denaturing conditions to visualize ssDNA.

K Quantification of (J). Fold change of nuclear BrdU signal relative to siLUC is shown. Error bars represent standard deviation and derive from three independent experiments.

L HeLa cells were transfected with I-PpoI endonuclease and stained for MST2 and γH2AX. Fluorescence intensity profiles of MST2 (green) and γH2AX (red) signals across the HeLa nuclei are shown. Position of line scan indicated by the yellow line.

M Validation of the MST2 siRNA with western blot.

N HeLa cells treated with siLUCIFERASE (siLUC) or siMST2 and 48 h later transfected with I-PpoI mRNA. Cells were treated with 5-EU for 30 min prior to fixation and assessed for incorporation.

O Quantification of 5-EU intensity in siLUCIFERASE (siLUC) or siMST2 treated cells transfected with I-PpoI mRNA. Middle line represents the median and the boxes 25th and 75th percentiles. The whiskers mark the smallest and largest values. 100 values were analyzed in each condition.

P HeLa cells were treated with siLUCIFERASE (siLUC) or siMST2 and 48 h post-transfection cells were transfected with I-PpoI mRNA. 6 h post transfection cells were fixed and stained for RASSF1A (R1A) and γH2AX.

Q Quantification of (P). Error bars represent standard deviation and derive from three independent experiments.

R–W HeLa cells treated with siLUCIFERASE (siLUC) or siMST2 and 48 h later transfected with I-PpoI mRNA. Cells were stained for ATM-pS1981 (R), KAP1-pS824 (T) and RPA (V) and quantified (S, U, W). 108 values were in (S), 95 values in (U) and 100 values in (W) were analyzed.

Data information: DNA was stained with DAPI. Scale bars = 10 μm. *P*-values in (A, B, D, F, K and Q) were calculated using two-tailed Student's *t*-test. *P*-values in (I, O, S, U and W) were calculated using a Mann–Whitney test. * indicates *P* = 0.05–0.01, ** indicates *P* = 0.01–0.001, *** indicates *P* ≤ 0.001.

Source data are available online for this figure.

(Fig 5J and K). REV7, a component of the Rev7-Shieldin complex, known to act downstream of 53BP1 to inhibit end resection (Ghezraoui *et al*, 2018), also gets recruited to the nucleolar caps of damaged nucleoli (Fig EV4T). In REV7 depleted cells, we observe RASSF1A recruitment and robust establishment of RPA and ATM-pS1981 at nucleolar caps (Figs EV4U and EV5A and B). In agreement with the data previously presented here, downregulation of 53BP1 results in cells with compromised ATM-pS1981 signal at nucleolar caps, that, however, retain robust RPA establishment (Fig EV5A and B).

The above data suggest that RASSF1A is part of a downstream 53BP1 signaling branch that is separate from the 53BP1-Rev7-Shieldin axis and that knockdown of the upstream adaptor 53BP1 establishes a different landscape in rDNA break repair compared to ATM inhibition or RASSF1A depletion. We previously reported that RASSF1A protects stalled replication forks from extended resection via BRCA2 stabilization of RAD51 nucleofilaments (Pefani *et al*, 2014). This function of the scaffold could also contribute to the defective establishment of RPA/RAD51 at damaged nucleoli upon RASSF1A downregulation.

We previously showed a role for RASSF1A in activating MST2 in the nucleolar interior to promote the establishment of H2B-pS14 (Pefani *et al*, 2018). To understand whether regulation of nucleolar MST2 kinase activity is involved in RASSF1A recruitment to nucleolar caps or the subsequent establishment of local ATM activation, we first looked for MST2 kinase localization at damaged nucleoli. Consistently with our previous observations for H2B-pS14 intranucleolar localization (Pefani *et al*, 2018), MST2 is found at the nucleolar interior of damaged nucleoli and not at the nucleolar caps

where RASSF1A relocates together with persistent breaks (Fig 5L). MST2 knockdown (Figs 5M and EV5C) results in continued 5-EU incorporation in damaged nucleoli as previously described (Figs 5N and O); however, under the same depletion conditions, we did not observe any effect on RASSF1A nucleolar cap localization (Fig 5P and Q), ATM-pS1981 (Fig 5R and S), KAP1-pS824 (Fig 5T and U) or RPA establishment at nucleolar caps (Fig 5V and W). The above data suggest that RASSF1A function at the sites of rDNA breaks does not involve activation of the MST2 kinase.

RASSF1A depletion results in persistent breaks, rDNA copy number aberrations and reduced survival

To assess the impact of impaired ATM signal establishment at damaged nucleoli upon decreased RASSF1A expression, we monitored rDNA repair kinetics at the rDNA break sites. Indeed, RASSF1A knocked down cells retain a higher number of rDNA breaks 24 h following I-PpoI induction, indicative of defective repair (Figs 6A and EV5D). To examine whether persistent breaks observed in the absence of RASSF1A could affect cell survival, we studied radiosensitivity of RASSF1A knocked down cells. Cell viability was affected in a γIR dose-dependent manner in cells with reduced RASSF1A expression (Fig 6B). Previous studies have highlighted the toxicity of rDNA breaks and their impact in cell survival (Warmerdam *et al*, 2016). To examine whether loss of RASSF1A also affects cell viability in the context of enriched DNA damage in the nucleolus, we performed clonogenic survival assays upon I-PpoI induced rDNA break formation. RASSF1A knockdown resulted in a significant reduction of cell viability in agreement with the scaffold

A

B

D

C

E

F
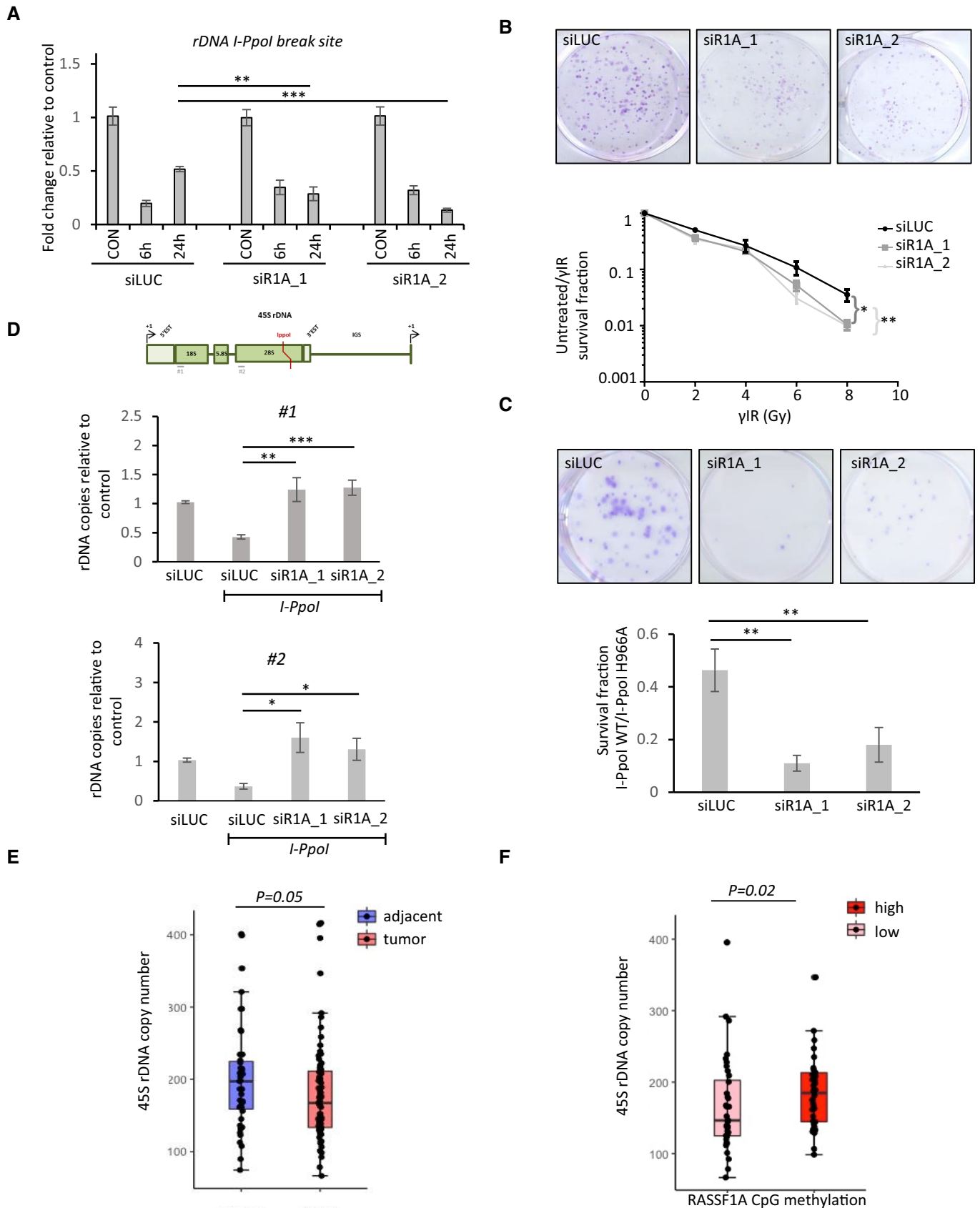
Figure 6.

◀

Figure 6. RASSF1A deletion results in reduced cell viability and rDNA copy number alterations.

A   HeLa cells were treated with the indicated siRNAs and 48 h later were transfected with I-PpoI mRNA to induce rDNA DSBs. Genomic DNA was isolated at the indicated time points post-mRNA transfection and quantitative real time PCR was performed with primers spanning the I-PpoI recognition site. Abundance of rDNA copies relative to control cells was quantified in each siRNA condition. Error bars represent standard deviation and derive from three independent experiments.

B   Clonogenic survival analysis of HeLa cells treated with the indicated siRNAs and the indicated doses of Ionizing radiation (γIR). Survival fraction was calculated. Error bars represent SEM and derive from three independent experiments.

C   Clonogenic survival analysis and representative images of HeLa cells treated with the indicated siRNAs followed by I-PpoI WT or I-PpoI H98A mRNA transfections. Survival ratio I-PpoI WT/I-PpoI H98A in each siRNA condition is presented. Error bars represent standard deviation and derive from three independent experiments.

D   Schematic representation of the 45S rDNA repeat. The I-PpoI cutting site and the binding sites of the primers used are shown. HeLa cells were treated with the indicated siRNAs and transfected or not with I-PpoI mRNA. 96 h post-mRNA transfection, genomic DNA was isolated and the rDNA copy number in the I-PpoI WT transfected cells relative to I-PpoI H98A transfected cells was accessed by real-time PCR. Error bars represent standard deviation and derive from three independent experiments.

E   45S rDNA copy number analysis in patients' tumors compared to adjacent controls in the LUAD cohort. Sixty-seven tumor samples and 43 samples from adjacent tissue were analyzed.

F   45S rDNA copy number analysis in the LUAD patient samples based on RASSF1A CpG promoter methylation. Sixty-seven samples were analyzed.

Data information: *P*-values in (A, C and D) derive from two-tailed Student's *t*-test. *P*-values in (B) were calculated with two way-Anova. *P*-values in (E and F) derive from Wilcoxon signed-rank test. * indicates *P* = 0.05–0.01, ** indicates *P* = 0.01–0.001, *** indicates *P* ≤ 0.001.

having a role in promoting rDNA break repair (Fig 6C). Similar results were also obtained when knockdown of RASSF1A was tested in combination with the CX-5461 Pol I inhibitor that results in rDNA break formation (Fig EV5E). Downregulation of MST2 kinase also results in reduced survival (Fig EV5F) as we previously reported (Pefani *et al*, 2018), potentially due to failed Pol I inhibition upon induction of damage. Depletion of 53BP1 had a major impact on cell survival upon induction of rDNA damage, indicative of the upstream function of the protein in the regulation of the rDNA damage response (Fig EV5F).

Due to the highly repetitive nature of the 45S rDNA arrays, breaks within the repeats may lead to excessive recombination and aberrations in the number of rDNA repeats. It was previously reported that rDNA breaks induced by I-PpoI result in loss of rDNA repeats in an HR-dependent manner (Warmerdam *et al*, 2016). We performed qPCR analysis on genomic DNA isolated from cells that had undergone rDNA damage and were treated with control siRNA or siRNAs against RASSF1A. We noticed that in contrast to controls that show decreased rDNA copies, surviving cells with low levels of RASSF1A did not exhibit loss of rDNA copies following induction of rDNA DSBs (Fig 6D). Retention of rDNA copy number was also observed in cells depleted for BRCA1, a key HR protein (Prakash *et al*, 2015) (Fig EV5G). siMST2-treated cells show loss of rDNA repeats as observed in siLUCIFERASE-treated cells upon induction of rDNA damage, further supporting that RASSF1A has additional functions in rDNA repair to MST2 kinase activity regulation (Fig EV5H).

A recent study by Wang and Lemos in patient cohorts showed that in several cancers, 45S rDNA repeats are lost as a result of recombinogenic events due to the accumulation of genomic instability (Wang & Lemos, 2017). Epigenetic loss of RASSF1A expression via promoter methylation is a common early event in lung malignant transformation (Grawenda & O'Neill, 2015). To address the correlation of RASSF1A promoter methylation with 45S rDNA copy number discrepancies, we explored publicly available data from the lung adenocarcinoma cohort (LUAD) of The Cancer Genome Atlas from which we extracted tumor information with *RASSF1A* promoter CpG island methylation status using Genomic Data Commons Data portal. Previous analysis showed that LUAD tumor samples presented fewer copies of 45S rDNA repeats compared to adjacent tissue (Wang & Lemos, 2017). We similarly observed 45S

repeat loss in the fraction of LUAD samples for which we had information on both RASSF1A promoter methylation status and 45S rDNA copy number (tumor = 67/adjacent = 43) (Fig 6E). We then sought to address the correlation of RASSF1A promoter methylation with 45S rDNA copy number alterations in the tumor samples. We analyzed the fractional methylation of a total 463 samples from the LUAD cohort and 63 samples of adjacent tissue, for which RASSF1A promoter methylation data were available, to set a cutoff for «high» and «low» methylation samples (Fig EV5I). «Highly» methylated are considered the samples that cluster higher than normal tissue RASSF1A promoter methylation levels. Tumor samples with fractional RASSF1A promoter methylation > 0.198 are listed as «highly methylated» and tumor samples with fractional methylation < 0.12 are listed as «low methylated». We observed a higher number of 45S rDNA repeats in the RASSF1A highly methylated tumors compared to the low methylated samples (Fig 6F), indicative of retention of rDNA copies in those tumors. This is in agreement with the hypothesis that RASSF1A facilitates Homologous-mediated repair, a driver of rDNA copy number loss, via local ATM signal establishment (Stults *et al*, 2009; Warmerdam *et al*, 2016; Wang & Lemos, 2017). We hypothesize that cells that have lost RASSF1A expression mostly rely on NHEJ for repair that takes place at the nucleolar interior (Harding *et al*, 2015).

Taken together, the above data identify the RASSF1A scaffold as a DNA repair factor that localizes at DSBs. We find RASSF1A in a subset of breaks and characterize recruitment to rDNA breaks. To our knowledge, this is the first report of endogenous RASSF1A localizing at the sites of DNA damage. rDNA loci are emerging fragile sites, and the nucleolar DNA damage response aims to secure efficient repair with reduced occurrence of translocations due to clustering of the repeats. We found that RASSF1A recruitment to rDNA sites depends on ATM activity and interaction with 53BP1. RASSF1A is necessary for MST2 kinase activation at the nucleolar interior for subsequent downregulation of Pol I transcription (Pefani *et al*, 2018). MST2 kinase does not relocate to the nucleolar caps or affect RASSF1A recruitment to the sites of damage. Moreover, MST2 knockdown does not phenocopy the perturbed establishment of ATM signaling evident in RASSF1A siRNA-treated cells. Therefore, we propose a model in which RASSF1A acts as a multifunctional adaptor during rDNA break repair via regulation of MST2 activity to establish H2BS14 phosphorylation in the nucleolar interior (Pefani

et al, 2018), and recruitment to persistent rDNA breaks in a 53BP1-dependent manner to facilitate local ATM signal establishment for efficient break repair (Fig 7). RASSF1A epigenetic inactivation, a process often observed during malignant transformation, fails to establish a local nucleolar DDR, leads to persistent breaks and increased genomic instability further supporting the role of the scaffold as a tumor suppressor.

Discussion

In this study, we provide evidence that RASSF1A adaptor acts as a *bona fide* DNA repair factor that accumulates at DSBs. We and others have previously shown the involvement of the scaffold in the maintenance of genome stability via or independently of the Hippo cascade (Pefani *et al*, 2014; Donninger *et al*, 2015). However, this is the first study to identify endogenous RASSF1A at the break sites colocalizing with DNA DSB markers. We find RASSF1A in a subset of γH2AX foci induced by γIR or radiomimetic agents and robust recruitment to the nucleolar periphery, where rDNA breaks relocate for homology mediated repair. We also observed that a fraction of RASSF1A[+ve] foci is not linked with the nucleoli, indicating that RASSF1A also marks other sites of damage. In future studies would be interesting to examine whether these sites could be non-active rDNA repeats that localize outside the nucleoli and have been recently reported (Potapova *et al*, 2019), or include other repetitive

elements (e.g., telomeric or centromeric repeats). Induction of breaks within a cassette that contains an I-SceI recognition sequence next to the LacO sequence integrated at two random chromosomal locations (Burgess *et al*, 2014) does not result in RASSF1A recruitment, suggesting that the chromatin environment could be important for the recruitment of the scaffold (Jeggo *et al*, 2017).

We previously showed that RASSF1A is involved in the nucleolar DNA damage response via regulation of MST2 kinase activity, that phosphorylates nucleolar H2B at Serine 14 facilitating Pol I transcriptional repression. In cell fractionation experiments, RASSF1A was found in the nucleolus independent of the presence of damage (Pefani *et al*, 2018). Neither MST2 nor H2B-pS14 were localized at the γH2AX[+ve] caps of the damaged nucleoli, as they accumulate at the nucleolar interior (Pefani *et al*, 2018). H2B-pS14 could mark either rDNA repeats that do not move to the periphery upon nucleolar segregation or evicted histones that have been released in the nucleolar interior to allow repair (Hauer & Gasser, 2017). In this study, we identify a fraction of RASSF1A at rDNA DSBs that have relocated to the nucleolar exterior. Further analysis showed that RASSF1A gets phosphorylated upon rDNA DSB formation by ATM at Serine 131 and ATM signaling is required for recruitment to the rDNA breaks (Hamilton *et al*, 2009).

53BP1 adaptor is mostly studied as a resection inhibitory factor that promotes NHEJ during G1 phase of the cell cycle (Zlotorynski, 2018). 53BP1 has also an established, but less well understood, role in promoting local ATM signal amplification mostly studied

rDNA break formation
Transcriptional shut down

rDNA break repair
Transcriptional restart

rDNA break movement

Nucleosome with H2B-pS14

RPA

RAD51
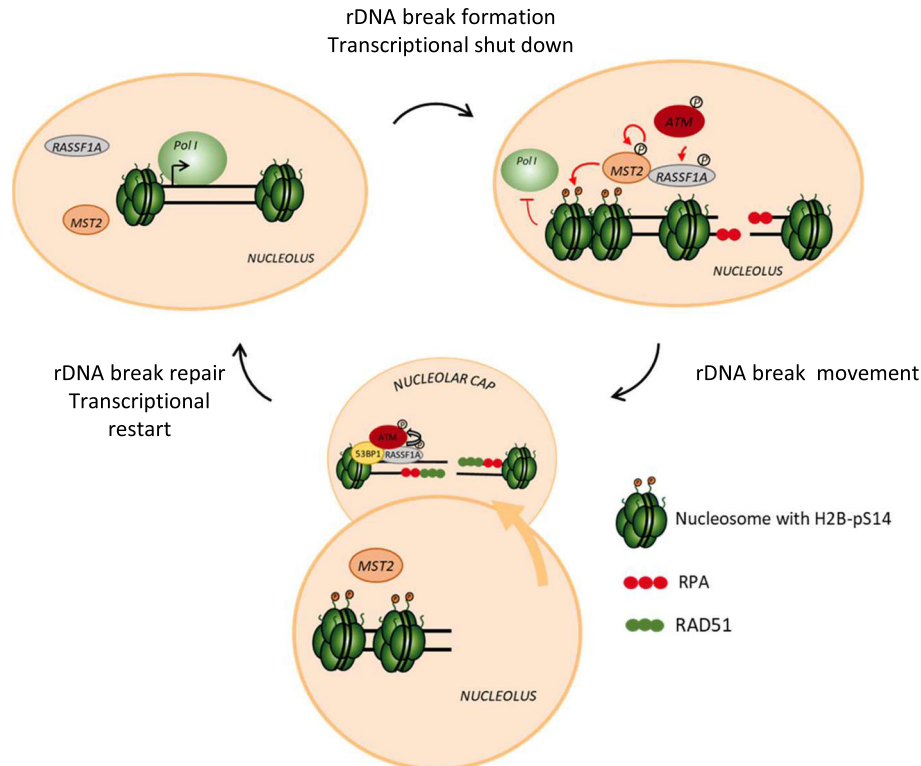
Figure 7. Model for the role of the RASSF1A scaffold in rDNA repair.

RASSF1A is a multifunctional protein that acts in the nucleolar DNA damage response via regulation of nucleolar chromatin dynamics in an MST2 kinase dependent manner in the nucleolar interior and rDNA break repair in a 53BP1 dependent manner at the nucleolar caps (see text for details).

within repetitive heterochromatic loci, where ATM-mediated phosphorylation of KAP1 at Serine 824 triggers chromatin relaxation (Mochan et al, 2003; Lee et al, 2010; Noon et al, 2010). ATM activity at γIR foci was shown to be stimulated by 53BP1 mediated interactions with MRN (Lee et al, 2010). Recent findings highlight that 53BP1 undergoes phase separation to integrate DNA repair factors in large repair compartments (Kilic et al, 2019). Liquid phase separation events are employed to achieve heterochromatin compartmentalization for break repair (Rawal et al, 2019) and are central in nucleolar organization (Feric et al, 2016). Therefore, 53BP1 could have a central role in organizing DNA repair at genetic loci where break movement is important to achieve repair.

We find RASSF1A to interact with 53BP1 upon rDNA DSB induction. Interaction between RASSF1A and 53BP1 requires ATM signaling as the RASSF1AS131A mutant showed reduced ability to bind to 53BP1. Moreover, a 53BP1 N-terminal deletion mutant that lacks the heavily ATM/ATR phosphorylated sites (Mirman & de Lange, 2020) is also necessary for interaction between the two adaptors. 53BP1 binds to the RASSF1A C-terminal SARAH domain, known to mediate interactions between Hippo pathway components including MST2-RASSF1A interaction (Sanchez-Sanz et al, 2016). RASSF1A interaction with 53BP1 is necessary for RASSF1A relocation to rDNA DSBs. We find that RASSF1A downregulation results in reduced local ATM signal establishment, a phenotype also observed upon depletion of the 53BP1 adaptor but not in response to MST2 knockdown. 5-EU incorporation is significantly increased in siMST2 treated cells, suggesting that lack of impact in ATM signal establishment is not due to residual kinase activity. Therefore, we propose a model in which induction of rDNA DSBs results in activation of pre-existing nucleolar pools of RASSF1A and MST2 in the nucleolar interior, promoting H2BS14 phosphorylation (Pefani et al, 2018). Following movement of persistent breaks to the nucleolar periphery and formation of DNA repair protein clusters at the nucleolar exterior, RASSF1A is recruited by 53BP1 at nucleolar caps where our data suggest that has a role in facilitating establishment of local ATM signals (Fig 7). SARAH-domain-mediated interaction with both MST2 and 53BP1 indicates a temporal mechanism with potentially "mutually exclusive" interactions. RASSF1A-MST2 interaction in the interior facilitates transcriptional shut down in response to rDNA breaks. Subsequent RASSF1A localization via 53BP1 to the caps where persistent breaks relocate facilitates their repair. Different RASSF1A pools (i.e., we show here that NE pools are recruited to rDNA breaks), or binding to different partners based on the presence of additional factors could also be involved in the regulation of the multifunctional role of the RASSF1A scaffold.

We also find that RASSF1A depletion results in impaired resection and decreased RPA establishment at nucleolar caps, a phenotype that mimics ATM inhibition (Korsholm et al, 2019; Mooser et al, 2020). Despite limited ATM-pS1981 establishment in cells depleted for 53BP1, we find robust RPA recruitment and accumulation of ssDNA at nucleolar caps, in agreement with its well-described role as an anti-resection factor. Moreover, depletion of BRCA1 results in enhanced 53BP1 signal at nucleolar caps, indicating that likewise to irradiation-induced foci, BRCA1 knockdown also results in enhanced 53BP1 recruitment to I-PpoI induced rDNA breaks (Feng et al, 2015). This data indicate that depletion of 53BP1, an upstream regulator of the nucleolar DNA damage response results in a different DNA repair landscape compared to

inhibition of downstream components. Moreover, concentrated ATM signaling appears to be dispensable for DNA end resection when 53BP1 is depleted. Further investigation of the significance of 53BP1 recruitment to nucleolar caps, a site where NHEJ does not take place and its impact on local ATM signal establishment, DNA end resection and repair pathway choice between HR or alternative end joining pathways (Microhomology Mediated End Joining/Single Strand Annealing) at nucleolar caps, would further improve our understanding of how the nucleolar DNA damage response is organized.

Translocation of the rDNA breaks has been proposed to serve in separating each NOR in a distinct nucleolar cap (Floutsakou et al, 2013). Break repositioning for homology mediated repair has been also observed in heterochromatic elements indicating that break mobilization is linked with repetitive element clustering (Chiolo et al, 2011; Jakob et al, 2011; Tsouroula et al, 2016; Mitrentsi et al, 2022). HR repair at rDNA loci often results in repeat loss (Warmerdam et al, 2016). In agreement with data derived from cell lines, in vivo studies in animal models and meta-analysis of TCGA panel tumors and normal tissue showed that genomic unstable cancers exhibit 45S rDNA repeat loss (Wang & Lemos, 2017; Xu et al, 2017). Loss of 45S rDNA repeats is considered a consequence of HR repair of breaks that derive from conflicts between transcription and replication in the rapidly dividing cancer cells. RASSF1A is frequently transcriptionally silenced in tumors due to promoter methylation an epigenetic event that associates with early cancer onset in lung cancer and correlates with adverse prognosis in several cancer types (Grawenda & O'Neill, 2015). We looked for copy number variations of 45S rDNA in a lung adenocarcinoma cohort (LUAD) and found that tumors with high levels of RASSF1A promoter methylation maintain a higher copy number compared to low promoter methylated lung cancers, an observation compatible with compromised HR rDNA repair. We also confirmed maintenance of rDNA repeats in cells in which RASSF1A expression is silenced after exposure to rDNA DSBs. We speculate that these cells possibly rely on NHEJ for repair that takes place fast after induction of damage in the nucleolar interior (Harding et al, 2015); however, alternative end joining pathways could also contribute to rDNA copy number discrepancies upon induction of rDNA breaks. We also observed a non-statistically significant trend of RASSF1A depleted damaged cells showing an increased number of rDNA copies compared to control cells, that could be attributed to endogenous rDNA damage accumulated prior to I-PpoI transfection.

Depletion of RASSF1A results in decreased cell viability upon induction of rDNA damage. Defective repair due to inadequate ATM signaling at nucleolar caps and persistent rDNA breaks evident in RASSF1A depleted cells could be responsible for compromised cell viability. Surviving cells potentially harbor extensive genomic instability to which they have probably adapted to, overcoming apoptosis checkpoints. Previous work has shown that RASSF1A can promote p73 mediated apoptosis in response to ATM signaling activation in a Hippo pathway dependent manner; therefore, RASSF1A loss could also facilitate escape from apoptosis of genomically unstable cells (Matallanas et al, 2007; Hamilton et al, 2009).

The challenging nature of the nucleoli constitutes a hub of genomic instability. Previous studies have highlighted differences in the regulation of the rDNA damage response compared to other genomic sites including dedicated adaptor proteins (Larsen

et al, 2014), differential regulation of ATM/ATR signaling (Korsholm et al, 2019; Mooser et al, 2020), repair of persistent breaks with HR through the cell cycle (van Sluis & McStay, 2015) and specific histone post-translational modifications (Pefani et al, 2018). Figuring out how the DNA damage response is organized in this area of the genome is important for understanding cancer development and designing novel cancer treatments. Nucleolar transcriptional activity and rDNA copy numbers have been proposed as biomarkers (Warmerdam & Wolthuis, 2019). CX-5461 Pol I inhibitor results in rDNA breaks due to stabilization of R-loops or G-quadruplexes and recombination deficient cancers showed increased sensitivity to the agent as a monotherapy or in combination with PARP inhibitors (Xu et al, 2017; Sanij et al, 2020). RASSF1A promoter methylation has been proposed as a biomarker in cancer diagnosis (Dubois et al, 2019). In this study, we provide additional mechanistic insight into rDNA DSB break repair and highlight the RASSF1A scaffold as DNA repair factor effectively recruited to rDNA breaks and important for the establishment of the local response.

Materials and Methods

Tissue culture and cell treatments

HeLa (ATCC), U2OS (ATCC) were cultured in complete DMEM and a-RPE19 (ATCC) in complete RPMI supplemented with 10% fetal bovine serum in 5% CO_2 and 20% O_2 at 37°C. DiVA U2OS cells stably expressing AsiSI-ER-AID (provided by Gaëlle Legube) were cultured in DMEM Glutamax. DSBs in DiVa cells were induced by the addition of 300 nM OHT (Sigma) for 4 h. U2OS cells with stable integration of the LacO-I-SceI-TetO cassette (provided by Vassilis Roukos) were grown in complete DMEM. Cells were transfected with plasmid DNA (2.5 μg/10^6 cells) or siRNA (50 nM) using Lipofectamine 2000 (Invitrogen) or Lipofectamine RNAiMAX (Invitrogen) according to the manufacturer's instructions. To introduce targeted DSBs in the rDNA, IGS gRNA (GATTTCCAGG-GACGGCGCCTTGG) was introduced in the pCAS9 vector (OriGene) and transfected in cells. I-PpoI WT and I-PpoI H98A mRNA transfections were conducted as previously described (van Sluis & McStay, 2015). In brief, plasmids were linearized at a NotI site and transcribed using the MEGAscript T7 kit (Ambion). I-PpoI mRNA was subsequently polyadenylated using a Poly(A) tailing kit (Ambion) according to the manufacturer's instructions. The in vitro transcribed mRNA was transfected using the TransMessenger transfection reagent (Qiagen) according to the manufacturer's instructions. Following 4 h of incubation, the transfection medium was replaced by full medium and cells were grown for additional 2 h unless stated otherwise. All irradiations were carried out using a Gamma Service® GSRD1 irradiator containing a Cs137 source. The dose rates of the system, as determined by the supplier, were 1.938 Gy/min and 1.233 Gy/min depending on the distance from the source. Cells were exposed in 5 Gy and fixed at the indicated time points. For the laser micro-irradiation experiments, cells seeded on ibidi glass bottom dishes (ibidi μ dish 35 mm 81156) were placed in an Olympus Cell-Vivo incubation chamber (37°C, 5% CO_2) and mounted on the stage of an Olympus IX-83 inverted widefield microscope. Micro-irradiation was performed by using a UV-A

pulsed laser (teemphotonics PNV-M02510- 355 nm- pulse < 350 ps) coupled to the epifluorescence path of the microscope which was focused to the sample through an Olympus Apochromat 63×/1.2 water immersion objective lens. Operation was assisted by the Rapp Optoelectronics software. Subnuclear irradiations were performed on a 10-μm linear ROI with the use of three pulses at 1% of the total laser power. After the laser micro-irradiation was performed, cells were incubated for 2 h in a normal cell culture incubator (37°C, 5% CO_2), unless stated otherwise and fixed and stained.

Drug treatments

The following inhibitors were used as follows: ATMi (KU55933 Selleck, 10 μM), ATRi (VE-821 Selleck, 10 μM), Pol Ii (CX-5461 Selleck, 1 μM), Neocarzinostatin (Sigma, 50 ng/μl). Cells were treated with ATM and ATR inhibitors for 1 h prior to I-PpoI mRNA transfections. Cells were treated with CX-5461 for 3 h. Cells were treated with NCS for 30 min and left to recover for 2 h before fixation.

Immunofluorescence

Cells were grown on coverslips and treated as indicated. Cells were fixed with 4% PFA at RT or with ice-cold Methanol at −20°C for 10 min, washed with 1× PBS, permeabilized with 0,5% Triton in 1x PBS and blocked with 2% BSA in 1× PBS. Coverslips were incubated with the indicated antibodies in blocking solution overnight at 4°C, washed and stained with secondary anti-rabbit and or anti-mouse IgG conjugated with Alexa Fluor secondary antibodies (Molecular Probes) for 1 h at RT. Coverslips were washed with PBS + 0.1% Tween, and DNA was stained with DAPI. For RASSF1A staining the HPA040735 from Atlas Antibodies was used. For BrdU staining under native conditions, cells were incubated with 10 μM BrdU for 24 h. Cells were then washed with ice-cold 1× PBS, pre-extracted on ice for 2 min with extraction buffer (10 mM PIPES pH 6.8, 100 mM NaCl, 300 mM Sucrose, 1.5 mM MgCl2 and 0.5% (v/v) Triton X-100) and fixed with ice-cold 4% PFA for 10 min. Cells were blocked with 10% FBS in 1× PBS, incubated with anti-BrdU antibody in 0.1% FBS in 1× PBS overnight at 4°C and stained with secondary antibody conjugated with Alexa Fluor for 1 h RT. DNA was stained with DAPI. Cells were analyzed using LSM780 (Carl Zeiss Microscopy Ltd) or Leica SP5 confocal microscopes. Image analysis was made using ImageJ software. In situ detection of nascent RNA was performed with the Click-iT Alexa Fluor 488 Imaging Kit (Invitrogen, Molecular Probes) after cells were treated with 0.5 mM 5-EU for 30 min. Cells were analyzed using LSM780 (Carl Zeiss Microscopy) or Leica LS5 confocal microscopes, and nuclear intensities were quantified with the NIS-elements software (Nikon).

Fluorescent in situ hybridization

FISH was performed as previously described (van Sluis et al, 2016). Briefly, cells were grown in sterile glass coverslips, fixed with 4% PFA, washed with 1× PBS, permeabilized with 0.5% Saponin/0.5% Triton in 1× PBS, washed with 1× PBS, incubated with 20% glycerol/PBS for 2 h RT and snap frozen in dry ice for 5 min. After thawing in RT, cells were denatured with 0.1 N HCl, washed with 2xSSC and incubated with 50% formamide/2xSSC for 15 min at 37°C. An rDNA probe (human rDNA plasmid pUC-

hrDNA-12.0: containing 12 kb that correspond between 30.5 and 42.5 kb of the rDNA repeat, provided by Brian McStay) diluted in a hybridization buffer (Hybrizol® VII) was placed on a slide and covered with the coverslip with the cells facing down and sealed with rubber cement. The slides were denatured at 85 °C for 5 min on a heat block and hybridization was carried out at 37°C for 18 h in an incubator with humidity. Cells were washed with 50% formamide/2xSSC at 42°C, and 0.1xSSC (prewarmed at 60°C) and DNA was stained with DAPI. When FISH was combined with immunofluorescence for UBF (ImmunoFISH), immunofluorescence was performed after FISH as described above. When FISH was combined with immunofluorescence for ATM-pS1981, ATM-pS1981 immunostaining was performed prior to FISH, cells were then fixed with 2% PFA, underwent FISH refixed with 2% PFA and stained with DAPI.

Immunoprecipitation

Cells were treated as indicated and washed with ice-cold 1× PBS prior to lysis. Cells were lysed in 1% NP-40 lysis buffer (150 mM NaCl, 20 mM HEPES, 0.5 mM EDTA) containing complete protease and phosphatase inhibitor cocktail (Roche) and 750 U/ml Benzonase (Millipore) and incubated for 30 min at 4°C. Cells lysates were sonicated, centrifuged at 13,000 rpm for 20 min and supernatants were incubated for 3 h with 20 µl protein A Dynabeads (Invitrogen) and 2 µg of RASSF1A antibody (Atlas, HPA040735), HA-tag (HA.C5, Millipore 05-904), MYC-tag (4A6, Millipore 05-724) or FLAG-tag (M2, Sigma, F3165) at 4°C. Total cell extracts (corresponding to 10% of the immunoprecipitate) and immunoprecipitates were analyzed by Western blotting.

Chromatin fractionation

Following indicated treatments, cells were harvested and the cytosolic fraction was removed by incubation with hypotonic buffer (10 mM HEPES, 10 mM KCl, 1.5 mM MgCl$_2$, 0.34 M sucrose, 10% glycerol and 0.1% Triton-X100 supplemented with protease and phosphatase inhibitors) for 10 min on ice following centrifuging. The pelleted nuclei were resuspended in nuclear buffer (10 mM HEPES, 3 mM EDTA, 0.2 mM EGTA, pH 8.0 supplemented with protease and phosphatase inhibitors) and nucleoplasm was released by centrifugation. The final pellet containing the chromatin fraction was resuspended in lysis buffer (10 mM HEPES, 500 mM NaCl, 1 mM EDTA, 1% NP-40, supplemented with protease and phosphatase inhibitor cocktails, Roche, and Benzonase, Millipore), sonicated three times at low amplitude, incubated on ice for 15 min and centrifuged to isolate the chromatin fraction. 10 µg of protein from the chromatin fraction were analyzed by Western blotting.

Western blotting

Extracts were analyzed by SDS–PAGE using a 4–12% Bis–Tris or 3–8% Tris-Acetate NuPAGE gels (Invitrogen) and transferred onto PVDF membranes (Millipore). After being washed with 1× PBS containing 1% Tween-20 (PBS-T), the membranes were blocked in 5% milk or 5% bovine serum albumin (BSA) in PBS-T for 1 h at RT and then incubated with the primary antibodies overnight at 4°C. The membranes were incubated with HRP-conjugated secondary

antibodies (Cell Signaling) for 1 h at RT and exposed to X-ray film (Kodak) or the ChemiDoc Imaging system (Biorad) after incubation with Thermo Scientific Pierce ECL or Clarity ECL (Biorad).

Quantitatively real-time PCR

Genomic DNA was extracted using the Nucleospin Genomic DNA from tissue kit (Machenrey-Nagel). Genomic DNA concentration and purity was measured using Nanodrop. rDNA copy number was assessed by quantitative real-time PCR (Applied Biosystems StepOne), using the PowerSYBR® mix (Ambion). rDNA copy number was quantified using the $2^{\Delta\Delta Ct}$ method relative to human GAPDH gene.

Clonogenic survival assays

Cells were transfected with the indicated siRNAs and 48 h post-transfection the appropriate number of cells was seeded in a well of a 6-well plates and treated with (i) the indicated doses of ionizing radiation by a Gamma Service® GSRD1 irradiator or (ii) with 100 nM CX5461 for 5 days. Cells were then grown for a remaining of 7–14 days in regular medium. Plates were then stained with crystal violet (0.5% w/v crystal violet, 50% v/v MeOH and 10% v/v EtOH). For clonogenic survival assays following rDNA DSBs, cells were treated with siRNAs and 48 h post-transfection, I-PpoI WT, or I-PpoI H98A mRNA was introduced with TransMessenger transfection reagent (Qiagen). 6 h post-mRNA transfection, cells were counted, and re-seeded in each well of a 6-well plates. Cells were grown for 10 days in regular medium and stained with crystal violet. Experiments were performed in triplicates. Survival fractions are presented corresponding to relevant viability of each siRNA condition with a DNA damage treatment relative to non-treated cells.

Antibodies

The following antibodies were used in this study: RASSF1A (1:100 in IF and 1:500 in WB, HPA040735, Atlas Antibodies), RASSF1A (1:300 in WB, 3F3, Santa Cruz, sc-58,470), pS131-RASSF1A (1:300 in WB) (Hamilton et al, 2009), V5 (1:1,000 in IF, 13202, Cell Signaling), γH2AX (1:1,000 in IF, JBW301, Millipore, 16–193), γH2AX (1:1,000 in IF and WB, 2577, Cell Signaling), Nucleolin (1:500 in IF, 4E2, ab13541, Abcam), Lamin A/C (1:1,000 in IF, 4777, Cell Signaling), 53BP1 (1:1,000 in IF and WB, NB100-304, Novus Biologicals), 53BP1 (1:500, B13, MAB3802, Millipore), MST2 (1:1,000, ab52641, Abcam), UBF (1:100 in IF, F9, sc-13,125, Santa Cruz), RNF8 (1:500 in IF and 1:1,000 in WB, 14112-1-A, Proteintech), RIF-1 (1:100 in IF, A300-569A, Bethyl Laboratories), RPA (1:1,000 in IF and WB, Ab2, NA18, Calbiochem), pRPAS33 (1:100 in WB, A300-246A, Bethyl Laboratories), pRPAS4/8 (1:1,000 in WB, A300-245A, Bethyl Laboratories), BRCA1 (1:100 in IF and 1:1,000 in WB, D-9, sc-6954, Santa Cruz), pATMS1981 (1:500 in IF, GeneTex, GTX61739), ATM (1:100 in IF, ab32420 Abcam), Treacle (1:200 in IF and 1:1,000 in WB, HPA038237, Atlas Antibodies), NBS1 (1:100 in IF, 1D7, GeneTex, GTX70224), NBS1 (1:100 in IF, 14956, Cell Signaling) RAD51 (1:100 in IF, 14B4, GTX70230, GeneTex), MRE11 (1:100 in IF, 12D7, ab214, Abcam), ATR (1:100 in IF, E1S3, Cell Signaling), Fibrillarin (1:200 in IF, Novus, NBP2-46881), REV7 (1:200 in IF and 1:1,000 in WB, ab180579, Abcam), BrdU (1:50 in IF, B44, BD Biosciences,

347580), pKAP1S824 (1:100 in IF and 1:1,000 in WB, ab70369, Abcam), KAP1 (1:1,000 in WB, 20C1, ab22553, Abcam), GAPDH (1:3,000 in WB, D4C6R, Cell Signaling, 97166), HA-tag (1:1,000 in WB, HA.C5, Millipore, 05-904), MYC-tag (1:000 in WB and IF, 4A6, Millipore 05-724) or FLAG-tag (1:1,000 in WB, M2, Sigma, F3165).

Correlation analysis

Methylation data for each patient were downloaded from the GDC portal of the TCGA website (portal.gdc.cancer.gov/projects/TCGA-LUAD). Only data relating to adenocarcinoma were selected, and out of these, methylation data were available for 526 patients. The RASSF1A CpG promoter region was defined as the region on chromosome 3 prior to and spanning exon1α. This region is on chr3:50,340,373–50,341,109 using GRCh38/hg38 (Malpeli *et al*, 2019) and contains 85 CpGs, 14 of which are detected using the Illumina 450 K array. The mean of the methylation frequencies (the ratio of methylated CpG to total CpG for each site in the dataset) across the 14 sites was used as a readout for RASSF1A methylation. Datasets containing rDNA copy numbers were kindly provided by Dr Wang (Harvard) and were calculated as described in (Wang & Lemos, 2017). All processing of data was performed using R Studio, Version 1.2.5033. Criteria for the selection of cutoff methylation frequencies for each analysis are as described in the results section.

Statistics

All experiments were performed three times unless otherwise specified in the figure legends. Error bars represent the standard deviation unless stated otherwise. Where statistical tests were applied, 75–200 cells were analyzed. For statistical analysis, unpaired two-tailed Student's *t*-test was used unless stated otherwise in the figure legend. For the rDNA analysis in the LUAD cohort, Wilcoxon signed-rank test was used. Statistical significance is depicted with stars (* = 0.05–0.01, ** = 0.01–0.001, *** $\leq$ 0.001).

Plasmids

pIRES V5 I-PpoI and pIRES V5 I-PpoI H98A were previously described (van Sluis & McStay, 2015). FLAG-RASSF1A and FLAG-RASSF1AS131A were previously described (Hamilton *et al*, 2009). HA-53BP1WT (aa1-1972), HA-53BP1ΔBRCT (aa 1–1709), HA-53BP1ΔNterminus (aa 921–1972) were previously described (Hansen *et al*, 2016). Myc-Tagged RASSF1A deletion mutants were previously described (Pefani *et al*, 2016). LacR-mCherry was previously described (Burgess *et al*, 2014). GFP-NLS-HA-I-SceI was constructed by inserting the HA-I-SceI fragment (Roukos *et al*, 2013) in frame with GFP in the pEGFPC1 plasmid (Clontech).

siRNA sequences:

Target gene	siRNA sequence
siLUCIFERASE	GCCAUUCUAUCCUCUAGAGGAUG
siRASSF1A_1	GACCUCUGUGGCGACUUCA
siRASSF1A_2	CACGUGGUGCGACCUCUGU
si53BP1	GGACUCCAGUGUUGUCAUUUU
siRNF8	siGENOME smartpool:M-006900-01 (Dharmacon)

Reagents and Tools table   (continued)

Target gene	siRNA sequence
siMST2	siGENOME smartpool: M-004874-02 (Dharmacon)
siBRCA1	siGENOME smartpool: M-003461-02 (Dharmacon)
siTreacle	CCACCAUGGGUUGGAACUAAAUU
siREV7	siGENOME smartpool: M-003272-03 (Dharmacon)

DNA oligos:

Target gene	DNA oligo sequence
I-PpoI rDNA:	Forward: 5'-GCCTAGCAGCCGACTTAGAA-3' Reverse: 5'-CTCACCGGGTCAGTGAAAAA-3'
I-PpoI rDNA:	Forward: 5'-AACGGCGGGAGTAACTATGA-3' Reverse: 5'-TAGGGACAGTGGGAATCTCG-3'
#1 rDNA primer (18S)	Forward: 5'-ACCACATCCAAGGAAGGCAG-3' Reverse: 5'-CGCTATTGGAGCTGGAATTAC-3'
#2 rDNA Primer (28S)	Forward: 5'-TGGAGCAGAAGGGCAAAAGC-3' Reverse: 5'-TAGGAAGAGCCGACATCGAAGG-3'
GAPDH	Forward: 5'-TACTAGCGGTTTTACGGGCG-3' Reverse: 5' -TCGAACAGGAGGAGCAGAGAGCG- 3'

Data availability

This study does not include data deposited in external repositories.

Expanded View for this article is available online.

Author contributions

Stavroula Tsaridou: Formal analysis; validation; investigation; visualization; methodology. **Georgia Velimezi:** Formal analysis; investigation; methodology. **Frances Willenbrock:** Formal analysis; investigation; visualization; methodology. **Maria Chatzifrangkeskou:** Investigation; methodology. **Waheba Elsayed:** Investigation; methodology. **Andreas Panagopoulos:** Investigation; visualization; methodology. **Dimitris Karamitros:** Resources; investigation; methodology. **Vassilis, G Gorgoulis:** Resources. **Zoi Lygerou:** Resources;

Disclosure and competing interest statement

References

Baldock RA, Day M, Wilkinson OJ, Cloney R, Jeggo PA, Oliver AW, Watts FZ, Pearl LH (2015) ATM localization and heterochromatin repair depend on direct interaction of the 53BP1-BRCT2 domain with gammaH2AX. *Cell Rep* 13: 2081−2089

Burgess RC, Burman B, Kruhlak MJ, Misteli T (2014) Activation of DNA damage response signaling by condensed chromatin. *Cell Rep* 9: 1703−1717

Chapman JR, Barral P, Vannier JB, Borel V, Steger M, Tomas-Loba A, Sartori AA, Adams IR, Batista FD, Boulton SJ (2013) RIF1 is essential for 53BP1-dependent nonhomologous end joining and suppression of DNA double-strand break resection. *Mol Cell* 49: 858−871

Chatzifrangkeskou M, Pefani DE, Eyres M, Vendrell I, Fischer R, Pankova D, O'Neill E (2019) RASSF1A Is required for the maintenance of nuclear Actin levels. *EMBO J* 38: e101168

Chiolo I, Minoda A, Colmenares SU, Polyzos A, Costes SV, Karpen GH (2011) Double-strand breaks in heterochromatin move outside of a dynamic HP1a domain to complete recombinational repair. *Cell* 144: 732−744

Clouaire T, Rocher V, Lashgari A, Arnould C, Aguirrebengoa M, Biernacka A, Skrzypczak M, Aymard F, Fongang B, Dojer N *et al* (2018) Comprehensive mapping of histone modifications at DNA double-Strand breaks deciphers repair pathway chromatin signatures. *Mol Cell* 72: e256

Daley JM, Sung P (2014) 53BP1, BRCA1, and the choice between recombination and end joining at DNA double-strand breaks. *Mol Cell Biol* 34: 1380−1388

DiTullio RA Jr, Mochan TA, Venere M, Bartkova J, Sehested M, Bartek J, Halazonetis TD (2002) 53BP1 functions in an ATM-dependent checkpoint pathway that is constitutively activated in human cancer. *Nat Cell Biol* 4: 998−1002

Donninger H, Clark J, Rinaldo F, Nelson N, Barnoud T, Schmidt ML, Hobbing KR, Vos MD, Sils B, Clark GJ (2015) The RASSF1A tumor suppressor regulates XPA-mediated DNA repair. *Mol Cell Biol* 35: 277−287

Dubois F, Bergot E, Zalcman G, Levallet G (2019) RASSF1A, puppeteer of cellular homeostasis, fights tumorigenesis, and metastasis-an updated review. *Cell Death Dis* 10: 928

El-Kalla M, Onyskiw C, Baksh S (2010) Functional importance of RASSF1A microtubule localization and polymorphisms. *Oncogene* 29: 5729−5740

Fages J, Chailleux C, Humbert J, Jang SM, Loehr J, Lambert JP, Cote J, Trouche D, Canitrot Y (2020) JMJD6 participates in the maintenance of ribosomal DNA integrity in response to DNA damage. *PLoS Genet* 16: e1008511

Feng L, Li N, Li Y, Wang J, Gao M, Wang W, Chen J (2015) Cell cycle-dependent inhibition of 53BP1 signaling by BRCA1. *Cell Discov* 1: 15019

Feric M, Vaidya N, Harmon TS, Mitrea DM, Zhu L, Richardson TM, Kriwacki RW, Pappu RV, Brangwynne CP (2016) Coexisting liquid phases underlie nucleolar subcompartments. *Cell* 165: 1686−1697

Floutsakou I, Agrawal S, Nguyen TT, Seoighe C, Ganley AR, McStay B (2013) The shared genomic architecture of human nucleolar organizer regions. *Genome Res* 23: 2003−2012

Ghezraoui H, Oliveira C, Becker JR, Bilham K, Moralli D, Anzilotti C, Fischer R, Deobagkar-Lele M, Sanchiz-Calvo M, Fueyo-Marcos E *et al* (2018) 53BP1 cooperation with the REV7-shieldin complex underpins DNA structure-specific NHEJ. *Nature* 560: 122−127

Gibbons JG, Branco AT, Godinho SA, Yu S, Lemos B (2015) Concerted copy number variation balances ribosomal DNA dosage in human and mouse genomes. *Proc Natl Acad Sci USA* 112: 2485−2490

Gorgoulis VG, Pefani DE, Pateras IS, Trougakos IP (2018) Integrating the DNA damage and protein stress responses during cancer development and treatment. *J Pathol* 246: 12−40

Grawenda AM, O'Neill E (2015) Clinical utility of RASSF1A methylation in human malignancies. *Br J Cancer* 113: 372−381

Hamilton G, Yee KS, Scrace S, O'Neill E (2009) ATM regulates a RASSF1A-dependent DNA damage response. *Curr Biol* 19: 2020−2025

Hansen RK, Mund A, Poulsen SL, Sandoval M, Klement K, Tsouroula K, Tollenaere MA, Raschle M, Soria R, Offermanns S *et al* (2016) SCAI promotes DNA double-strand break repair in distinct chromosomal contexts. *Nat Cell Biol* 18: 1357−1366

Harding SM, Boiarsky JA, Greenberg RA (2015) ATM dependent silencing links nucleolar chromatin reorganization to DNA damage recognition. *Cell Rep* 13: 251−259

Hauer MH, Gasser SM (2017) Chromatin and nucleosome dynamics in DNA damage and repair. *Genes Dev* 31: 2204−2221

Ide S, Miyazaki T, Maki H, Kobayashi T (2010) Abundance of ribosomal RNA gene copies maintains genome integrity. *Science* 327: 693−696

Jackson SP, Bartek J (2009) The DNA-damage response in human biology and disease. *Nature* 461: 1071−1078

Jakob B, Splinter J, Conrad S, Voss KO, Zink D, Durante M, Lobrich M, Taucher-Scholz G (2011) DNA double-strand breaks in heterochromatin elicit fast repair protein recruitment, histone H2AX phosphorylation and relocation to euchromatin. *Nucleic Acids Res* 39: 6489−6499

Jeggo PA, Downs JA, Gasser SM (2017) Chromatin modifiers and remodellers in DNA repair and signalling. *Philos Trans R Soc Lond Ser B Biol Sci* 372: 20160279

Kilic S, Lezaja A, Gatti M, Bianco E, Michelena J, Imhof R, Altmeyer M (2019) Phase separation of 53BP1 determines liquid-like behavior of DNA repair compartments. *EMBO J* 38: e101379

Kleiner RE, Verma P, Molloy KR, Chait BT, Kapoor TM (2015) Chemical proteomics reveals a gammaH2AX-53BP1 interaction in the DNA damage response. *Nat Chem Biol* 11: 807−814

Korsholm LM, Gal Z, Lin L, Quevedo O, Ahmad DA, Dulina E, Luo Y, Bartek J, Larsen DH (2019) Double-strand breaks in ribosomal RNA genes activate a distinct signaling and chromatin response to facilitate nucleolar restructuring and repair. *Nucleic Acids Res* 47: 8019−8035

Kruhlak M, Crouch EE, Orlov M, Montano C, Gorski SA, Nussenzweig A, Misteli T, Phair RD, Casellas R (2007) The ATM repair pathway inhibits RNA polymerase I transcription in response to chromosome breaks. *Nature* 447: 730−734

Larsen DH, Hari F, Clapperton JA, Gwerder M, Gutsche K, Altmeyer M, Jungmichel S, Toledo LI, Fink D, Rask MB *et al* (2014) The NBS1-treacle complex controls ribosomal RNA transcription in response to DNA damage. *Nat Cell Biol* 16: 792−803

Lee JH, Goodarzi AA, Jeggo PA, Paull TT (2010) 53BP1 promotes ATM activity through direct interactions with the MRN complex. *EMBO J* 29: 574–585

Lindstrom MS, Jurada D, Bursac S, Orsolic I, Bartek J, Volarevic S (2018) Nucleolus as an emerging hub in maintenance of genome stability and cancer pathogenesis. *Oncogene* 37: 2351–2366

Mailand N, Bekker-Jensen S, Faustrup H, Melander F, Bartek J, Lukas C, Lukas J (2007) RNF8 ubiquitylates histones at DNA double-strand breaks and promotes assembly of repair proteins. *Cell* 131: 887–900

Malpeli G, Innamorati G, Decimo I, Bencivenga M, Nwabo Kamdje AH, Perris R, Bassi C (2019) Methylation dynamics of RASSF1A and its impact on cancer. *Cancers (Basel)* 11: 959

Marnef A, Finoux AL, Arnould C, Guillou E, Daburon V, Rocher V, Mangeat T, Mangeot PE, Ricci EP, Legube G (2019) A cohesin/HUSH- and LINC-dependent pathway controls ribosomal DNA double-strand break repair. *Genes Dev* 33: 1175–1190

Matallanas D, Romano D, Yee K, Meissl K, Kucerova L, Piazzolla D, Baccarini M, Vass JK, Kolch W, O'Neill E (2007) RASSF1A elicits apoptosis through an MST2 pathway directing proapoptotic transcription by the p73 tumor suppressor protein. *Mol Cell* 27: 962–975

Mirman Z, de Lange T (2020) 53BP1: a DSB escort. *Genes Dev* 34: 7–23

Mitrentsi I, Lou J, Kerjouan A, Verigos J, Reina-San-Martin B, Hinde E, Soutoglou E (2022) Heterochromatic repeat clustering imposes a physical barrier on homologous recombination to prevent chromosomal translocations. *Mol Cell* 82: 2132–2147

Mitrentsi I, Yilmaz D, Soutoglou E (2020) How to maintain the genome in nuclear space. *Curr Opin Cell Biol* 64: 58–66

Mochan TA, Venere M, DiTullio RA Jr, Halazonetis TD (2003) 53BP1 and NFBD1/MDC1-Nbs1 function in parallel interacting pathways activating ataxia-telangiectasia mutated (ATM) in response to DNA damage. *Cancer Res* 63: 8586–8591

Mooser C, Symeonidou IE, Leimbacher PA, Ribeiro A, Shorrocks AK, Jungmichel S, Larsen SC, Knechtle K, Jasrotia A, Zurbriggen D *et al* (2020) Treacle controls the nucleolar response to rDNA breaks via TOPBP1 recruitment and ATR activation. *Nat Commun* 11: 123

Noon AT, Shibata A, Rief N, Lobrich M, Stewart GS, Jeggo PA, Goodarzi AA (2010) 53BP1-dependent robust localized KAP-1 phosphorylation is essential for heterochromatic DNA double-strand break repair. *Nat Cell Biol* 12: 177–184

Pefani DE, Latusek R, Pires I, Grawenda AM, Yee KS, Hamilton G, van der Weyden L, Esashi F, Hammond EM, O'Neill E (2014) RASSF1A-LATS1 signalling stabilizes replication forks by restricting CDK2-mediated phosphorylation of BRCA2. *Nat Cell Biol* 16: 962–971

Pefani DE, O'Neill E (2016) Hippo pathway and protection of genome stability in response to DNA damage. *FEBS J* 283: 1392–1403

Pefani DE, Pankova D, Abraham AG, Grawenda AM, Vlahov N, Scrace S, O'Neill E (2016) TGF-beta targets the hippo pathway scaffold RASSF1A to facilitate YAP/SMAD2 nuclear translocation. *Mol Cell* 63: 156–166

Pefani DE, Tognoli ML, Pirincci Ercan D, Gorgoulis V, O'Neill E (2018) MST2 kinase suppresses rDNA transcription in response to DNA damage by phosphorylating nucleolar histone H2B. *EMBO J* 37: e98760

Potapova TA, Unruh JR, Yu Z, Rancati G, Li H, Stampfer MR, Gerton JL (2019) Superresolution microscopy reveals linkages between ribosomal DNA on heterologous chromosomes. *J Cell Biol* 218: 2492–2513

Prakash R, Zhang Y, Feng W, Jasin M (2015) Homologous recombination and human health: The roles of BRCA1, BRCA2, and associated proteins. *Cold Spring Harb Perspect Biol* 7: a016600

Rawal CC, Caridi CP, Chiolo I (2019) Actin' Between phase separated domains for heterochromatin repair. *DNA Repair (Amst)* 81: 102646

Rong R, Jin W, Zhang J, Sheikh MS, Huang Y (2004) Tumor suppressor RASSF1A is a microtubule-binding protein that stabilizes microtubules and induces G2/M arrest. *Oncogene* 23: 8216–8230

Roukos V, Voss TC, Schmidt CK, Lee S, Wangsa D, Misteli T (2013) Spatial dynamics of chromosome translocations in living cells. *Science* 341: 660–664

Sanchez-Sanz G, Matallanas D, Nguyen LK, Kholodenko BN, Rosta E, Kolch W, Buchete NV (2016) MST2-RASSF protein-protein interactions through SARAH domains. *Brief Bioinform* 17: 593–602

Sanij E, Hannan KM, Xuan J, Yan S, Ahern JE, Trigos AS, Brajanovski N, Son J, Chan KT, Kondrashova O *et al* (2020) CX-5461 activates the DNA damage response and demonstrates therapeutic efficacy in high-grade serous ovarian cancer. *Nat Commun* 11: 2641

Schwertman P, Bekker-Jensen S, Mailand N (2016) Regulation of DNA double-strand break repair by ubiquitin and ubiquitin-like modifiers. *Nat Rev Mol Cell Biol* 17: 379–394

van Sluis M, McStay B (2015) A localized nucleolar DNA damage response facilitates recruitment of the homology-directed repair machinery independent of cell cycle stage. *Genes Dev* 29: 1151–1163

van Sluis M, van Vuuren C, McStay B (2016) The relationship between human nucleolar organizer regions and nucleoli, probed by 3D-ImmunoFISH. *Methods Mol Biol* 1455: 3–14

Stults DM, Killen MW, Pierce HH, Pierce AJ (2008) Genomic architecture and inheritance of human ribosomal RNA gene clusters. *Genome Res* 18: 13–18

Stults DM, Killen MW, Williamson EP, Hourigan JS, Vargas HD, Arnold SM, Moscow JA, Pierce AJ (2009) Human rRNA gene clusters are recombinational hotspots in cancer. *Cancer Res* 69: 9096–9104

Tsouroula K, Furst A, Rogier M, Heyer V, Maglott-Roth A, Ferrand A, Reina-San-Martin B, Soutoglou E (2016) Temporal and spatial uncoupling of DNA double Strand break repair pathways within mammalian heterochromatin. *Mol Cell* 63: 293–305

Wang M, Lemos B (2017) Ribosomal DNA copy number amplification and loss in human cancers is linked to tumor genetic context, nucleolus activity, and proliferation. *PLoS Genet* 13: e1006994

Warmerdam DO, van den Berg J, Medema RH (2016) Breaks in the 45S rDNA Lead to recombination-mediated loss of repeats. *Cell Rep* 14: 2519–2527

Warmerdam DO, Wolthuis RMF (2019) Keeping ribosomal DNA intact: A repeating challenge. *Chromosom Res* 27: 57–72

Xu H, Di Antonio M, McKinney S, Mathew V, Ho B, O'Neil NJ, Santos ND, Silvester J, Wei V, Garcia J *et al* (2017) CX-5461 is a DNA G-quadruplex stabilizer with selective lethality in BRCA1/2 deficient tumours. *Nat Commun* 8: 14432

Xu B, Li H, Perry JM, Singh VP, Unruh J, Yu Z, Zakari M, McDowell W, Li L, Gerton JL (2017) Ribosomal DNA copy number loss and sequence variation in cancer. *PLoS Genet* 13: e1006771

Zlotorynski E (2018) Shieldin the ends for 53BP1. *Nat Rev Mol Cell Biol* 19: 346–347